The Institute of Space and Astronautical Science
Report No. 645, June 1992

Monte Carlo Calculation of Ionization and Excitation Rates in Electron Aurora

By

Kunizo ONDA,[*1] Makoto HAYASHI,[*2] and Kazuo TAKAYANAGI[*3]

(April 23, 1992)

Ionization and excitation of atmospheric N_2, O and O_2 in electron aurora are studied numerically in the Monte Carlo approach. Electrons are assumed to be injected downward into the upper atmosphere at the altitude of 250 km. The initial electron energy is 3, 5 or 7.5 keV. Time variation of the energy- and altitude-distribution of the electrons (primary and secondary electrons) is studied and the numbers of various collision processes are counted. Particularly, the number of photo-emission of the first-negative band system of molecular nitrogen and the red and green lines of atomic oxygen, and the number of ion-electron pairs created are found as functions of the altitude. The continuous-slowing-down (CSD) approximation, which was used earlier in the same problem by one of the present authors (K.T.), is tested. In the intensity of the above-mentioned photo-emissions and the ionization rate as functions of the height, good agreement is obtained between the Monte Carlo and the CSD calculations, except in the lowest region of the altitude.

1. INTRODUCTION

Aurorae are produced by charged particles precipitating from outside the atmosphere. The charged particles are mainly electrons and protons. The mechanism of production, acceleration and precipitation of these charged particles is one of the most interesting subjects of study in magnetospheric physics. Other important features of aurorae are the excitation of various emissions and the production of atmospheric ionization by the precipitating particles. Study of these features is a problem of radiation physics and an application of atomic and molecular collision physics. The main features of the ultraviolet, visible and infrared spectra of aurorae are summarized, for instance, in the recent article by Vallance Jones and Gattinger [*1*].

The charged particles are accelerated in magnetosphere up to the energy range from a few to about 10 keV. In this energy range, electrons are fast and produce a large number of ionization, excitation and molecular dissociation in the atmosphere, while protons in the same energy range are rather slow and

*[1]Associate member
*[2]ISAS Visiting professor from 1984 to 1985. Professor emeritus of Nagoya Institute of Technology. Present address: Gaseous Electronics Institute, Sakae High-Home No. 503, 15-14, Sakae 4-chome, Naka-ku, Nagoya 460
*[3]Professor emeritus. Present address: Faculty of Systems Engineering, Shibaura Institute of Technology, Fukasaku, Omiya, Saitama-ken 330

major collision processes other than the elastic one are the charge transfer processes. Therefore, electron aurorae have a much larger variety of atomic and molecular processes. In this paper, we study electron aurorae.

If the structure of the atmosphere (chemical composition, number density and temperature as functions of altitude), magnetic field, and the initial condition of the precipitating electrons (energy and pitch-angle distributions and the total flux as functions of time) were precisely given, the application of any authentic method of approach in radiation physics would give ionization and radiative emission rates which should be in good agreement with observations. However, the initial condition of the precipitating particles changes from aurora to aurora, while the structure of the atmosphere also changes from time to time, although the time scale in the latter is much longer. Furthermore, the accurate cross section data are not necessarily available for all the relevant collision processes. Therefore, it is not possible to quantitatively test the theoretical models by comparing with observations. The largest variability is in the initial energy distribution and the flux of the incident electrons. Some people try to use the observed intensity ratio of some emission lines to infer the energy distribution of the precipitating electrons through the comparison of the observed values with model calculations (Richards and Torr [2] and references therein).

Coordinated experiments are sometimes carried out where the flux and the energy distribution of the incident electrons are measured in situ by a satellite, while the ionization increase in the ionosphere and the intensity of some line emissions downstream are measured by the same or another satellite or by a sounding rocket. However, natural auroral activities change quickly, temporally and spatially, so that it is rather difficult to determine simultaneously all the relevant parameters with sufficiently high accuracy and resolution.

If an aurora is produced artificially by injection of electrons with known energy distribution from a space vehicle into atmosphere, it will give us a good opportunity to test theoretical models. SEPAC (Space Experiment with Particle Accelerator) was designed as one of the experiments in the first spacelab program onboard an American space shuttle. The flight took place from November 28 to December 8 in 1983. Unfortunately, the experiment was unsuccessful because of an unexpected failure of the apparatus. When the date of that SEPAC experiment came nearer, one of the present authors (K.T.) started some model calculations to help analysis of the data to be obtained. The calculations were based on the continuous-slowing-down (CSD) approximation for the precipitating electrons. The results of the work were published in 1984 [3]. Later, the same experiment was re-scheduled in another space shuttle program. At that time, we planned to start more accurate calculations. The purpose of the work is twofold. First, it is to predict the ionization increase and the intensity of some radiative emissions in the coming artificial aurora experiment. Secondly, it is to test the accuracy of the CSD approximation.

For the transport of precipitating electrons, there have been many theoretical calculations (Banks et al. [4], Strickland *et al.* [5], Stamnes [6], Richards and Torr [2]). Usually, the transport equation is solved to determine the electron

flux as a function of energy, pitch angle and altitude. Various kinds of approximation are often introduced. In the so-called two-stream model, for instance, a set of equations is derived for hemispherical fluxes of two electron streams (upward and downward) and solved. The discreteness of the collision processes is not taken into account explicitly in these calculations.

Our calculations, which are reported in the present paper, are based on the Monte Carlo method. This approach was used by Berger *et al.* [7] for studying the precipitation of energetic electrons from the height of 300 km. However, they did not calculate the emission rates.

Outline of the calculation method used in the present work is described in the next section (2). For the atmospheric structure, we have chosen one from the CIRA models in 1972 [8]. For the collision cross sections, the data set used in the previous work (Takayanagi [3]) was replaced by a more recent data compilation, although the difference between the two sets is not large. The results of calculations are reported in 3, while summary and discussions are given in the last section (4).

The re-scheduled space shuttle experiment has been postponed many times and it is being carried out in March 1992, while we are finalizing this report. We hope that the experiment has been a successful one and gives us an opportunity to test the present work as well as the other model calculations of ionization and optical excitation efficiencies for electron precipitation.

2. Outline of the Monte Carlo Calculations

In the present work, the behavior of an electron is simulated on computer. For a given initial condition (altitude, energy and pitch angle), such a calculation is repeated a large number of times. All the results for a common initial condition are summed up to see the spread of electron swarm in time and in space. Motion of the secondary electrons produced in ionizing processes is also traced and their contribution to further ionization and excitation is estimated.

In real aurorae, a large number of electrons come down together. There may be the cases where the space charge and the plasma waves have important influence on the motion of individual electrons. These effects are ignored in the present study.

2.1 Electron Trajectory between Collisions

Within the range of altitude of our interest, i.e., from 100 to 250 km, the geomagnetic line of force will be approximately regarded as straight. The z axis of our coordinate system will be taken along the line of force. The motion of an electron (mass m, charge q) will be determined by solving the classical equation of motion:

$$m\, d\boldsymbol{v}/dt = q\boldsymbol{F} + q\boldsymbol{v} \times \boldsymbol{B}, \tag{1}$$

where $\boldsymbol{v}$ is the electron velocity, $\boldsymbol{F}$ and $\boldsymbol{B}$ are the electric and magnetic fields, respectively. The MKS units have been used. In the present work, however, the electric field is neglected. The solutions for the electron velocity $\boldsymbol{v} = (v_x, v_y, v_z)$ and the electron position $\boldsymbol{r} = (x, y, z)$ in components are given by

$$v_x = v_\perp \cos \omega_B t \tag{2a}$$

$$v_y = v_\perp \sin \omega_B t \tag{2b}$$

$$v_z = v_{z0} \tag{2c}$$

$$x = (v_\perp/\omega_B)\sin \omega_B t + x_0 \tag{3a}$$

$$y = -(v_\perp/\omega_B)\cos \omega_B t + y_0 \tag{3b}$$

$$z = v_{z0} t + z_0, \tag{3c}$$

where the suffix "0" indicates the initial value, and ω_B is the Larmor frequency

$$\omega_B = qB/m. \tag{4}$$

In (2a, b), (3a, b), $v_\perp$ is the component of velocity perpendicular to the line of force. The radius of gyration is given by

$$a = v_\perp/\omega_B = mv_\perp/qB. \tag{5}$$

The formulae (3a, b, c) are used to describe the electron motion during free flights.

2.2 Treatment of Collision Processes

(A) *Decision of Occurrence of Collision*

Let N_j be the number density of atoms or molecules of the jth component of the atmosphere. The total collision cross section of this component for an incident electron with energy E will be designated as $\sigma_T(j; E)$. Every time after the electron has moved by a small, specified distance Δl, the decision will be made about the occurrence of collision. The procedure of the decision is as follows. The probability of collision of an electron in the distance Δl is given by

$$P_{\Delta l} = \sum_{j=1}^{N_G} N_j(x,y,z)\ \sigma_T(j;\ E)\Delta l, \tag{6}$$

where N_G is the number of components of the atmosphere. Now a small constant number ε is chosen in the range (0, 1), and the step length Δl is chosen as

$$\Delta l = \varepsilon \Big/ \sum_{j=1}^{N_G} N_j(x,y,z)\ \sigma_T(j;\ E). \tag{7}$$

Then, the probability of collision (6) becomes

$$P_{\Delta l} = \varepsilon. \tag{8}$$

In the present work, the number ε will be taken as $\varepsilon = 0.1$, based on the experience of one of the authors (M.H.) in similar calculations in gaseous electronics. The time Δt spent by the electron passage by the distance Δl is given by

$$\Delta t = \varepsilon \Big/ \bar{v} \sum_{j=1}^{N_G} N_j(x,y,z)\ \sigma_T(j;\ E). \tag{9}$$

where $\bar{v}$ is the mean velocity in the time interval Δt. Thus the decision of the occurrence of collision will be made at time Δt after the previous decision. Now a random number ξ_C ($0 \leq \xi_C \leq 1$) is created on computer and decision will be made as follows:

$$\begin{aligned} &\text{If} \quad \xi_C \leq \varepsilon, \text{ collision takes place.} \\ &\text{If} \quad \xi_C > \varepsilon, \text{ no collision takes place.} \end{aligned} \tag{10}$$

(B) *Decision of Type of Collision Target*

Suppose that the precipitating electron collides with a target of the jth kind. The effective cross section for a specified type of collision process "k" will be designated as $\sigma_k\ (j;\ E)$. The sum of σ_k over k gives $\sigma_T\ (j;\ E)$. Elastic collision will be represented by $k = 1$, ionization by $k = N_k$, while $k = 2, 3, \ldots, N_k-1$ represent excitations to discrete levels. For N_2, however, we distinguish the three lowest states of N_2^+ in the ionization product in order to estimate the emission rate for the first negative bands. Thus, for N_2, $k = N_k-2$, N_k-1 and N_k

correspond to the production of the lowest three states of N_2^+ in ionization, respectively. Furthermore, it is noted that for the elastic collision we use the momentum-transfer cross section because elastic collisions with small scattering angles need not be regarded as "collisions" in the present problem.

Now we introduce a weight function:

$$W(E;\ x,y,z) = \sum_j w_j(E;\ x,y,z), \tag{11a}$$

$$w_j(E;\ x,y,z) = \sigma_T(j;\ E)\ N_j(x,y,z). \tag{11b}$$

A number ξ_G is randomly created in the range [0, 1], and the decision is made as follows:

$$\left.\begin{aligned} &\text{If}\quad \xi_G \le w_1 / W, \text{ the collision target is } j = 1. \\ &\text{If}\quad w_1 / W < \xi_G \le (w_1+w_2) / W, \text{ the target is } j = 2. \\ &\qquad\qquad \cdots\cdots\cdots\cdots \\ &\text{If}\quad (w_1+w_2+\ldots+w_{N_G-1}) / W < \xi_G, \text{ the target is } j = N_G. \end{aligned}\right\} \tag{12}$$

(C) *Decision of Type of Collision Process*

A random number ξ_K in the range [0, 1] is created and the collision type is decided as follows:

$$\text{If}\quad \xi_K \le \sigma_1(j;\ E)/\sigma_T(j;\ E), \text{ the collision is elastic.} \tag{13a}$$

$$\left.\begin{aligned} &\text{If}\ \frac{\sum_{k=1}^{I-1} \sigma_k(j;\ E)}{\sigma_T(j;\ E)} < \xi_K \le \frac{\sum_{k=1}^{I} \sigma_k(j;\ E)}{\sigma_T(j;\ E)},\ (I = 2, 3, \ldots, N_K-1), \\ &\text{the collision is the excitation of the } I\text{th kind. (In the case of } N_2, \\ &I \text{ runs from 2 to } N_K-3 \text{ for excitation and } I = N_K-2, N_K-1 \text{ correspond, respectively, to ionization producing } N_2^+(X^2\Sigma_g^+) \text{ and } N_2^+(A^2\Pi_u).) \end{aligned}\right\} \tag{13b}$$

If $\sum_{j=1}^{N_K-1} \sigma_k(j; E) / \sigma_T(j; E) < \xi_K$, the collision is an ionizing one.

(For N_2, this particularly corresponds to the production of $N_2^+(B^2\Sigma_u^+)$.) (13c)

(D) *Decision of the Scattering Direction*

The differential cross section for the relevant collision processes is known only fragmentarily, so that we assume rather arbitrarily that above $E = 200$ eV the scattering is predominantly forward (zero scattering angle), while below $E = 200$ eV the scattering is isotropic. In the latter, the direction of electron motion after scattering is chosen as follows:

The azimuthal angle χ is determined by a random number ξ_A in the range of [0, 1] as

$$\chi = 2\pi\xi_A. \tag{14}$$

The scattering angle, i.e., the angle between the velocity vectors before and after scattering, ω, is determined by

$$\cos \omega = 1 - 2\xi_p, \tag{15}$$

where ξ_p is another random number in the range [0, 1]. The unit vector $\hat{\boldsymbol{v}}'(\theta', \phi')$ along the initial velocity and the angles (ω, χ) determine the unit vector $\hat{\boldsymbol{v}}(\theta, \phi)$ along the final velocity as follows:

$$\cos \theta = \cos \theta' \cos \omega + \sin \theta' \sin \omega \cos \chi \tag{16a}$$

$$\sin \theta \cos \phi = \cos \phi'(\cos \omega \sin \theta' - \sin \omega \cos \theta' \cos \chi) + \sin \phi' \sin \omega \sin \chi \tag{16b}$$

$$\sin \theta \sin \phi = \sin \phi'(\cos \omega \sin \theta' - \sin \omega \cos \theta' \cos \chi) - \cos \phi' \sin \omega \sin \chi. \tag{16c}$$

(E) *Energy of Scattered Electron*

For an inelastic collision, the electron energy after collision is given by

$$E_f = E_i - \Delta E, \tag{17}$$

where E_i is the energy before collision and ΔE is the energy loss in the collision. For an ionizing collision, ΔE is sum of the relevant ionization energy and the kinetic energy of the secondary electron. For an elastic collision, energy loss is given by the momentum-transfer loss

$$\Delta E = \frac{2m}{M_j} (1 - \cos \omega) E_i, \tag{18}$$

where M_j is the mass of the jth particle.

(F) *Secondary-Electron Energy Distribution*

When the target is a molecule, N_2 or O_2, we use the approximate analytic expression (Opal *et al.* [9]) for the energy distribution:

$$f(\varepsilon) = \frac{C}{1 + (\varepsilon/\zeta)^{2.1}}, \tag{19}$$

where ε is the energy of the ejected electron, ζ is a constant (12.7 eV for N_2 and 17.5 eV for O_2) and C is the normalization constant. For the atomic oxygen, we have no experimental data for $f(\varepsilon)$. We use the same $f(\varepsilon)$ as for O_2.

2.3 Initial Condition for the Electron Precipitation

The initial condition is defined by the set of the following parameters:

1) altitude h_0 of the spot where the electrons were injected downward into atmosphere,

2) energy E_0 of the electrons,

3) pitch angle α, which is the angle between the initial electron velocity and the geomagnetic line of force.

In addition to these, we also need the value of

4) angle β between the local line of force and the vertical line.

As was mentioned already in the section 2.1, it is assumed that the line of force can be regarded straight within the range of altitude of our interest.

Values of these parameters chosen in the present work are:

$$h_0 = 250 \text{ km},$$

$$E_0 = 3 \text{ keV}, 5 \text{ keV}, \text{ and } 7.5 \text{ keV},$$

$$\alpha = 0° \text{ and } 60°,$$

$$\beta = 30° \text{ and } 60°.$$

2.4 Termination of the Calculation

As soon as the electron energy becomes below 5 eV, we stop tracing that electron.

2.5 Adopted Model of Atmosphere

The mean reference atmosphere with exospheric temperature T_{ex} = 800 K is adopted from CIRA(1972) [*8*]. As the atmospheric particles, only N_2, O and O_2 are taken into account in the present work. The adopted number densities and the temperature are shown in Figs. 1 and 2 as functions of the altitude.

2.6 Adopted Set of Collision Cross Sections

In addition to the momentum transfer in the elastic collisions, the excitation of discrete levels and the ionization with or without excitation of the residual ion are considered for each neutral component of the atmosphere. The states taken into account in the present work and the respective threshold energies are listed in Tables 1~3. As was mentioned in the section 2.2(C), three electronic states of N_2^+ are distinguished in ionizing collision of N_2. For O and O_2, however, we did not distinguish the ion states. Thus the ionization cross sections used for these targets include all the ionic products. And yet, we use the single threshold energy, i.e., the ionization energy for the lowest ion state all the time. The values of the relevant cross sections used in this work are those reported in the recent data reviews by Itikawa et al. [*10, 11*] and by Itikawa and Ichimura [*12*]. These data compilations include some more recently published data, so that the present data set is close to, but slightly different from those used in the previous work [*3*].

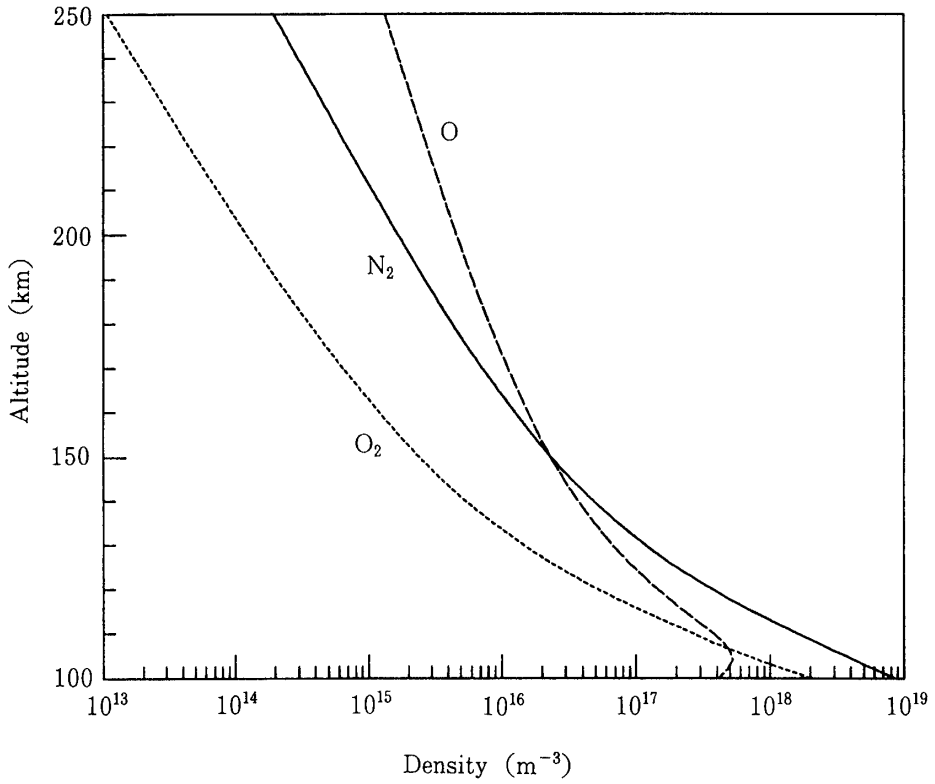

Fig. 1. Adopted distribution of neutral atmospheric particles.

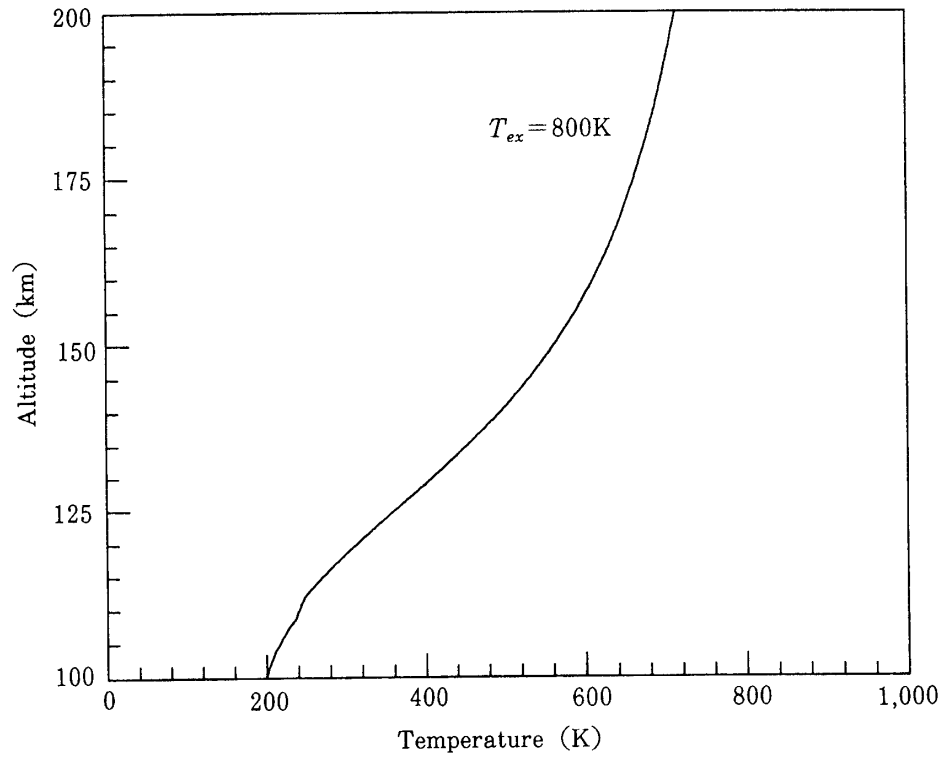

Fig. 2. Adopted atmospheric temperature

Table 1. Inelastic processes between electron and N_2

molecular states produced*)	$v = 1$	$v = 2$	$A^3\Sigma_u^+$	$B^3\Pi_g$	$W^3\Delta_u$	$B'^3\Sigma_u^-$
threshold energy (eV)	0.289	0.574	6.17	7.35	7.36	8.16

molecular states produced	$a'^1\Sigma_g^-$	$a^1\Pi_g$	$w^1\Delta_u$	$C^3\Pi_u$	$E^3\Sigma_g^+$	$a''^1\Sigma_g^+$
threshold energy (eV)	8.40	8.55	8.89	11.03	11.88	12.25

molecular states produced	sum of higher singlet states in 12.5-14.2eV	$N_2^+(X^2\Sigma_g^+)$	$N_2^+(A^2\Pi_u)$	$N_2^+(B^2\Sigma_u^+)$
threshold energy (eV)	13.0 (adopted)	15.6	17.0	18.8

*) v stands for the vibrational quantum number. The pure vibrational excitations $v = 0 \rightarrow 1, 2$ are taken into account in the collision energy range of 5 – 75 eV.

Table 2. Inelastic processes between electron and O

atomic states produced	$(2p)^4\ ^1D$	$(2p)^4\ ^1S$	$(2p)^3\ 3s\ ^5S$	$(2p)^3 3s\ ^3S$
threshold energy (eV)	1.967	4.190	9.146	9.521

atomic states produced	$(2p)^3 3p\ ^5P$	$(2p)^3 3p\ ^3P$	$(2p)^3 4s\ ^3S$	$(2p)^3 3d\ ^3D$
threshold energy (eV)	10.74	10.99	11.93	12.09

atomic states produced	$(2p)^3 4p\ ^5P$	$(2p)^3 4p\ ^3P$	$O^+((2p)^3\ ^4S, ^2D, ^2P)$
threshold energy (eV)	12.29	12.36	13.61

Table 3. Inelastic processes between electron and O_2

molecular states produced*)	$v = 1$	$v = 2$	$a^1\Delta_g$	$b^1\Sigma_g^+$	$A^3\Sigma_u^+ + C^3\Delta_u + c^1\Sigma_u^-$
threshold energy (eV)	0.193	0.383	0.982	1.64	6.1 (adopted)

molecular states produced	$B^3\Sigma_u^-$	sum of higher excited states in 9.7-12.1eV	O_2^+
threshold energy (eV)	8.5	9.7 (adopted)	12.1

*) The pure vibrational excitations are taken into account in the collision energy range of 5 – 20 eV. Besides the processes listed above, the dissociative attachment, where the free electron disappears, is also taken into account in the present calculations in the energy range below 12 eV, although the relative importance of this process is rather low.

A few words must be said about the excitation of the N_2 states in the range of 12.5-14.2 eV. In this range, most of the states excited by electron impact are singlet states. The excitation cross sections are reported only at collision energies of 40 and 60 eV [*13, 14*]. The sum of these cross sections has been interpolated or extrapolated rather arbitrarily and used in the previous work [*3*]. There is another set of data for this group of excited states recommended by Phelps and Pitchford [*15*]. These data are based on their analysis of electron swarm experiments. As is shown in Fig. 3, there is a considerable discrepancy between the two sets of effective cross sections. In this work, the two model cross sections *A* and *B* in Fig. 3 are adopted. It is seen later that the difference in the model cross sections does not give rise to any serious change in the total number of events of various kind. This is because most of the excitation and ionization processes are caused by the low-energy secondary electrons, for which the difference in the cross sections at higher energies is irrelevant. Most of the calculations reported here are based on the cross section curve B. Here is the major difference in cross sections used in the present work and in the previous work [*3*].

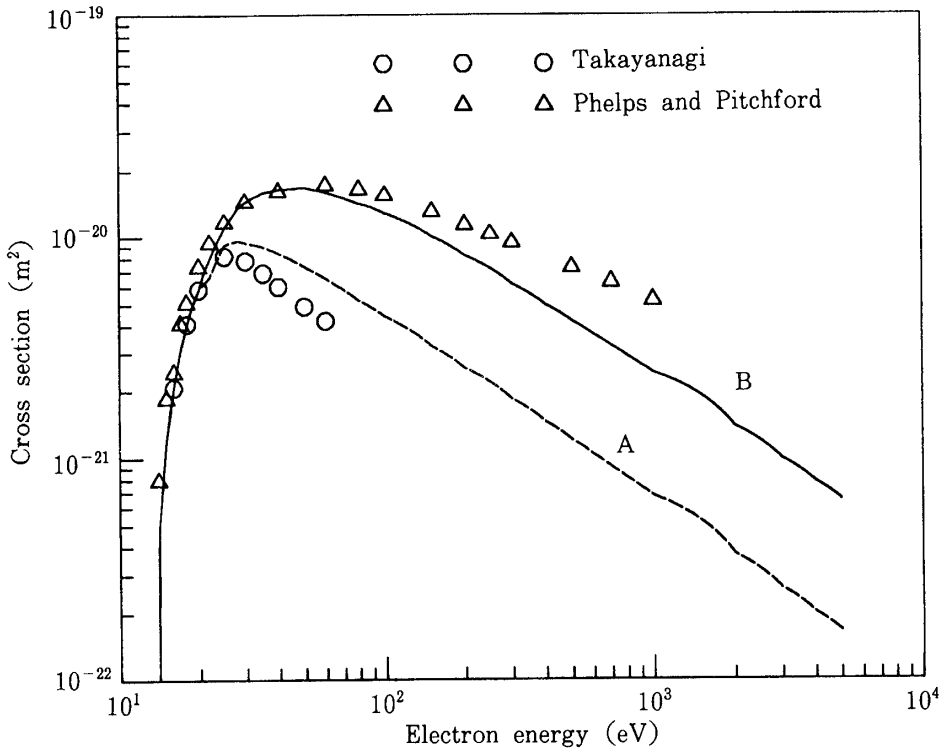

Fig. 3. Summed excitation cross sections of the higher singlet states of N_2. See text for explanation.

The cross section data are input into computer in numerical form at appropriately chosen energy values, including excitation threshold, maxima, minima, cusps, etc. of the relevant cross sections, and linearly interpolated for other energy values. For the excitation of N_2 to $A^3\Sigma_u^+$, for instance, cross section data at 29 energy values are input, while for O_2 $B^3\Sigma_u^-$ at 34 energy values, between the respective excitation threshold and a sufficiently high energy, such as 1 keV, 5 keV, 10 keV or 30 keV, depending on the process, where the cross section is assumed to be zero.

The energy loss of the precipitating electrons by collisions with ambient ionospheric electrons has been neglected in this work. This is permissible because the energy-loss rate due to this mechanism is orders of magnitude smaller than the energy loss by excitation of atoms and molecules in the atmosphere at least in the energy range above 5 eV.

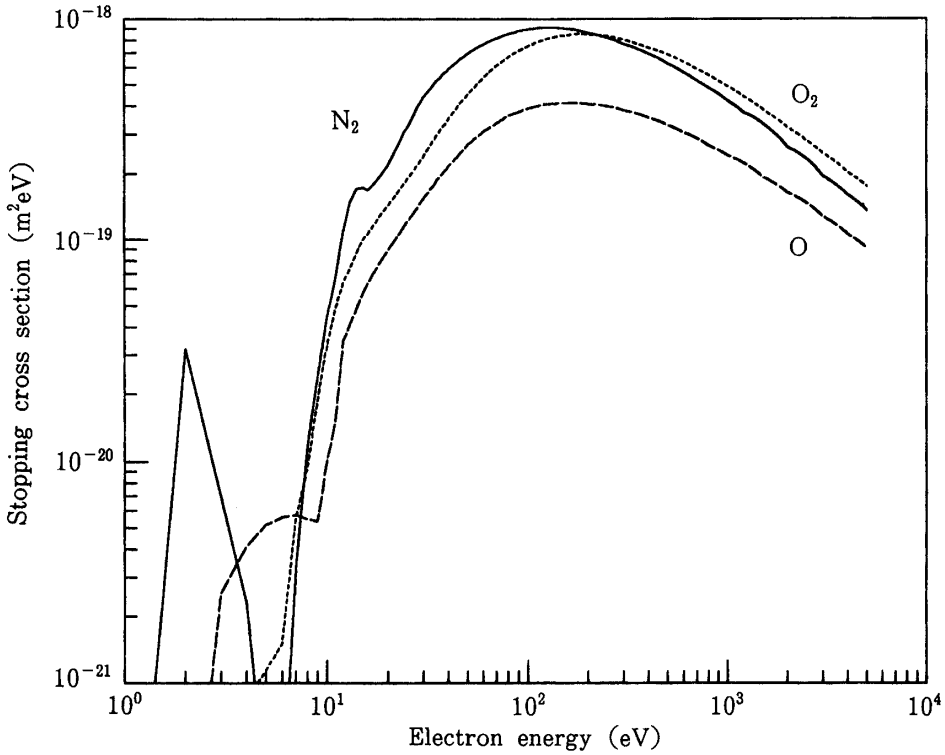

Fig. 4. Stopping cross sections for N_2, O and O_2. A sharp peak of N_2 in the low energy region is due to the resonant vibrational excitations. The well-known comblike structure has been smoothed by the use of a coarse energy mesh.

2.7. Continuous-Slowing-Down (CSD) Model

We shall compare the results of the Monte Carlo calculations with those obtained in CSD model, using the same set of cross section data. In this approximation model, the electron energy loss per unit height drop is given by

$$\frac{dE}{dh} = \sec\alpha \cdot \sec\beta \sum_{j,k} N_j(h) S_k(j; E), \tag{20}$$

where the stopping cross section S_k is given by

$$S_k(j; E) = \Delta E_{j,k}\, \sigma_k(j; E). \tag{21}$$

$\Delta E_{j,k}$ is the electron energy loss in the collision process of the type k with an atmospheric particle of the jth kind. It is seen that the angles α and β appear symmetrically in the formula. The total stopping cross section

$$S(j; E) = \sum_k S_k(j; E) \tag{22}$$

calculated by using our cross section sets is shown in Fig. 4 for N_2, O and O_2.

3. Results of Calculations

3.1 Dependence on the Excitation Cross Sections for the Higher Singlet States (HSS) of N_2

In the previous section, it has been shown that there is ambiguity in the excitation cross section for the N_2 states with the excitation energy in the range of 12.5-14.2 eV. Thus, we first perform two sets of Monte Carlo calculations, one with the model cross section A and the other with the model cross section B in Fig. 3. The resulting number of events for the initial energy E_0 = 5 keV, α = 0° and β = 30° is shown in Table 4 for various collision processes. It is seen that the two sets of numbers are fairly close to each other. Thus, the choice of the cross section among A and B is not a serious problem in the present calculations. In the rest of our calculations, we adopt the model cross section B.

3.2. Overall Picture of the Electron Precipitation

In deriving numbers in Table 4 and in all the other Monte Carlo calculations reported in this article, we have studied one thousand primary electrons and the secondary electrons produced therefrom for each set of parameters. In order to see the accuracy of this procedure, we also performed a larger size calculation for 2000 primary electrons in the case of $E_0 = 5$ keV, $\alpha = 0°$ and $\beta = 30°$. The number of events obtained in these two sets of calculations agree remarkably well when we compare the numbers per primary electron. In most processes, we have a difference less than one percent. Only in a small number of less important processes, the difference becomes two or three percent. Therefore, in the rest of calculations, only one thousand primary electrons were traced for each set of parameters.

Table 4. Number of various collision processes per primary electron for $E_0 = 5$ keV, $\alpha = 0°$ and $\beta = 30°$. *A* and *B* represent, respectively, the Monte Carlo calculations with the model cross sections *A* and *B* in Fig. 3.

N_2			O			O_2		
processes*)	*A*	*B*	processes*)	*A*	*B*	processes*)	*A*	*B*
MT	7.72(3)	6.99(3)	*MT*	8.72(2)	8.11(2)	*MT*	7.91(2)	7.13(2)**)
$v = 1$	3.88 (1)	3.50(1)	$(2p)^4\ ^1D$	5.04(1)	4.67(1)	$v = 1$	1.33(1)	1.20(1)
$A^3\Sigma^+_u$	2.95(1)	2.74(1)	$(2p)^4\ ^1S$	2.84	2.66	$a^1\Delta_g$	1.00(1)	9.13
$B^3\Pi_g$	2.23(1)	2.08(1)	$(2p)^3 3s\ ^3S$	1.65	1.53	$b^1\Sigma^+_g$	2.26	2.13
$W^3\Delta_u$	1.27(1)	1.18(1)	$(2p)^3 3p\ ^3P$	1.93	1.77	A+C+c	4.41	3.96
$a^1\Pi_g$	1.51(1)	1.37(1)	O^+	2.32(1)	2.20(1)	$B^3\Sigma^-_u$	9.61	8.60
HSS	3.37(1)	6.13(1)				*HS*	1.34	1.14
$N_2^+(X^2\Sigma^+_g)$	4.86(1)	4.47(1)				O_2^+	2.44(1)	2.19(1)
$N_2^+(A^2\Pi_u)$	7.30(1)	6.72(1)						
$N_2^+(B^2\Sigma^+_u)$	1.32(1)	1.21(1)						
total number of collisions	8.05(3)	7.32(3)	total number of collisions	9.55(2)	8.72(2)	total number of collisions	8.63(2)	7.77(2)

*) excited or ionized states produced. *MT* stands for momentum-transfer collision. *HSS* is the excitation of higher singlet states in the energy range of 12.5-14.2 eV. A+C+c means the sum of excitation of $A^3\Sigma^+_u$, $C^3\Delta_u$ and $c^1\Sigma^-_u$. *HS* is the higher excited states in O_2 in the energy range of 9.7-12.1 eV.

**) $7.13(2) = 7.13 \times 10^2$

Figs. 5a, b, c show the energy and altitude distributions of the primary electrons at 3, 4 and 5 ms after being injected into the atmosphere at the altitude of 250 km. The initial energy is 5 keV and the angles α and β are chosen to be 0° and 30°, respectively. The distribution is normalized to one electron. In Fig. 5a, the distribution consists of many discrete peaks or spikes. However, this result is an artifact. In higher altitudes, the atmospheric number density is extremely small. Furthermore, the collision cross section is also very small at 5 keV. Therefore, the mean free path is very large. It is over 60 km at the altitude of 200 km. This means that at 3 ms after the injection, electrons have experienced only a few collisions at most. Besides, in the present treatment, collisions take place only with specified time intervals. Under these conditions, the smoothing of the distribution function does not come until the later stages of the precipitation. Please note also that the ordinate is in different scale in the three figures. We have assumed that electrons are scattered into the forward direction (zero scattering angle) in collision processes as long as electron energy is over 200 eV. For α = 0°, therefore, electrons come down very quickly along the magnetic line of force. At 5 ms after the injection, almost all electrons are in the altitude region below 120 km.

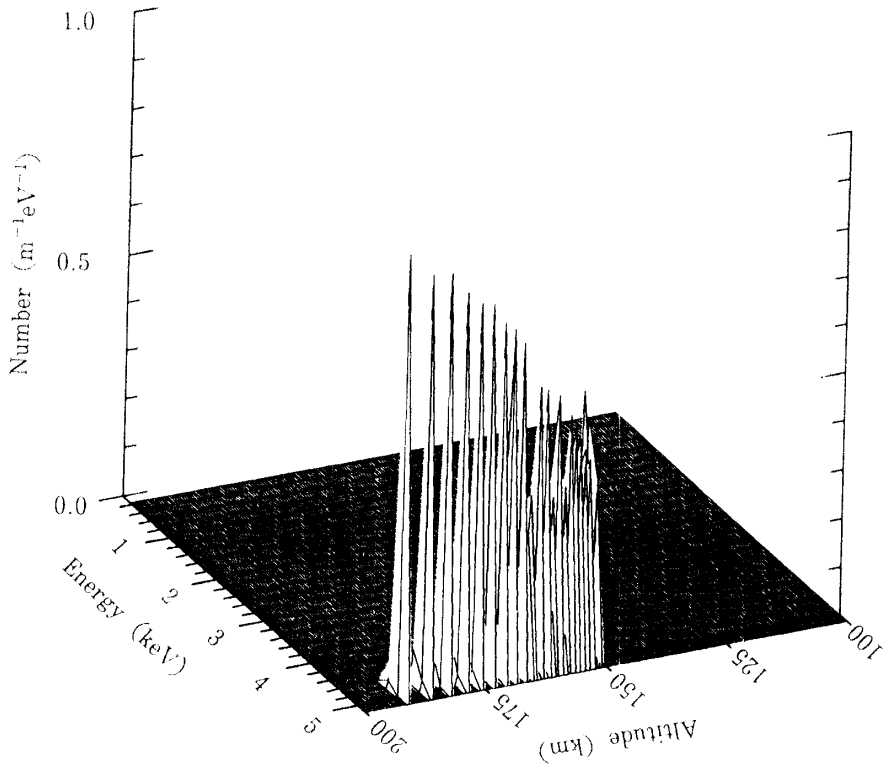

Fig. 5a. Energy and altitude distribution of the primary electrons injected with the initial energy E_0 = 5 keV. Angles are α = 0°, β = 30°. Distribution has been normalized to one electron. 3 ms after the injection at 250 km.

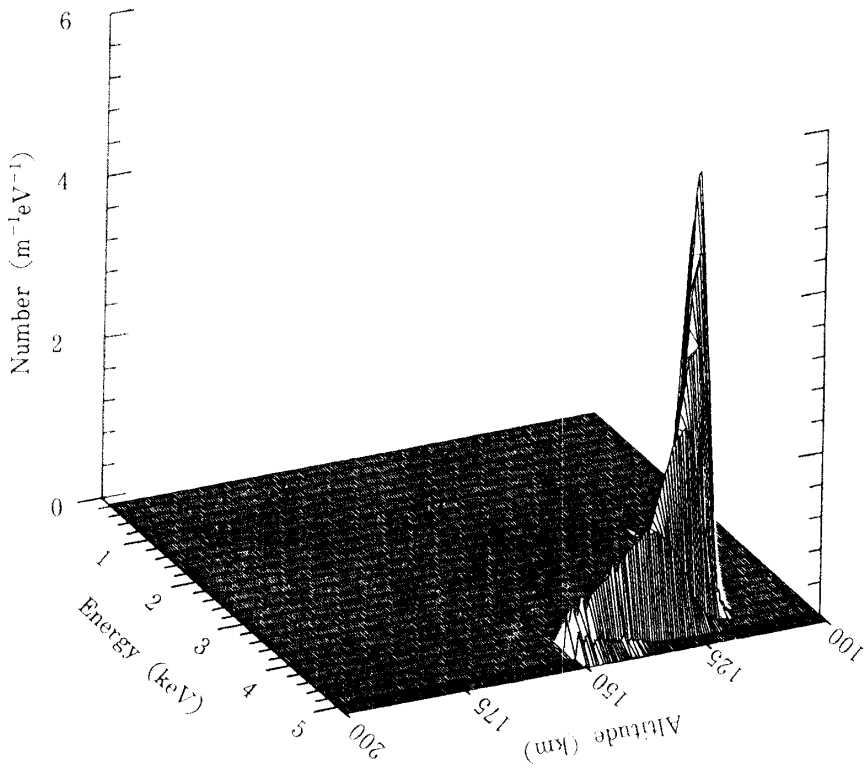

Fig. 5b. Same as Fig. 5a, but for 4 ms after the injection.

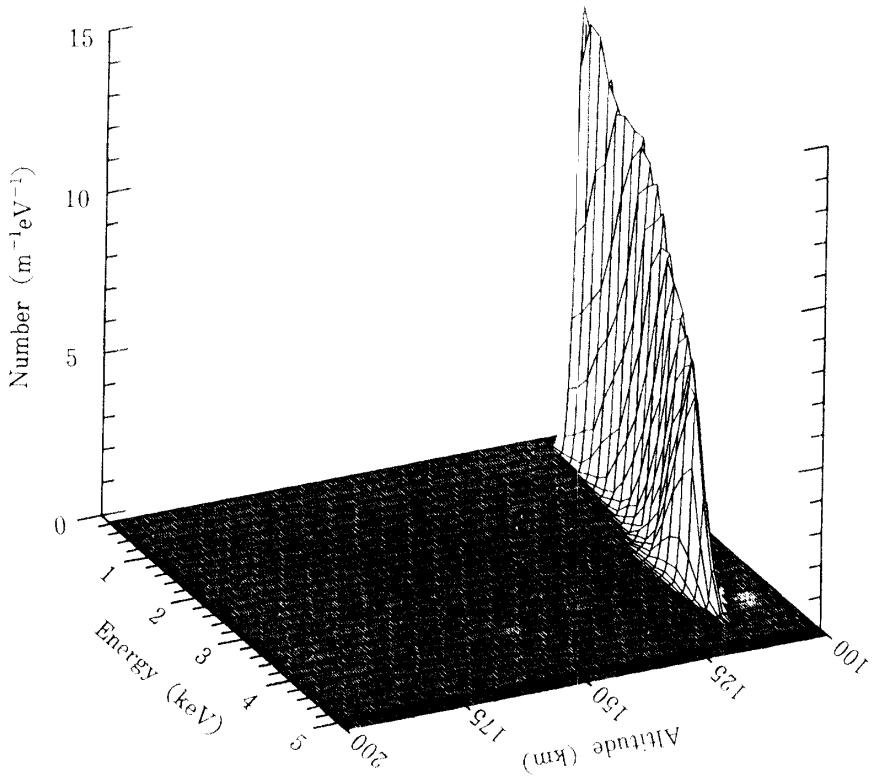

Fig. 5c. Same as Fig. 5a, but for 5 ms after the injection.

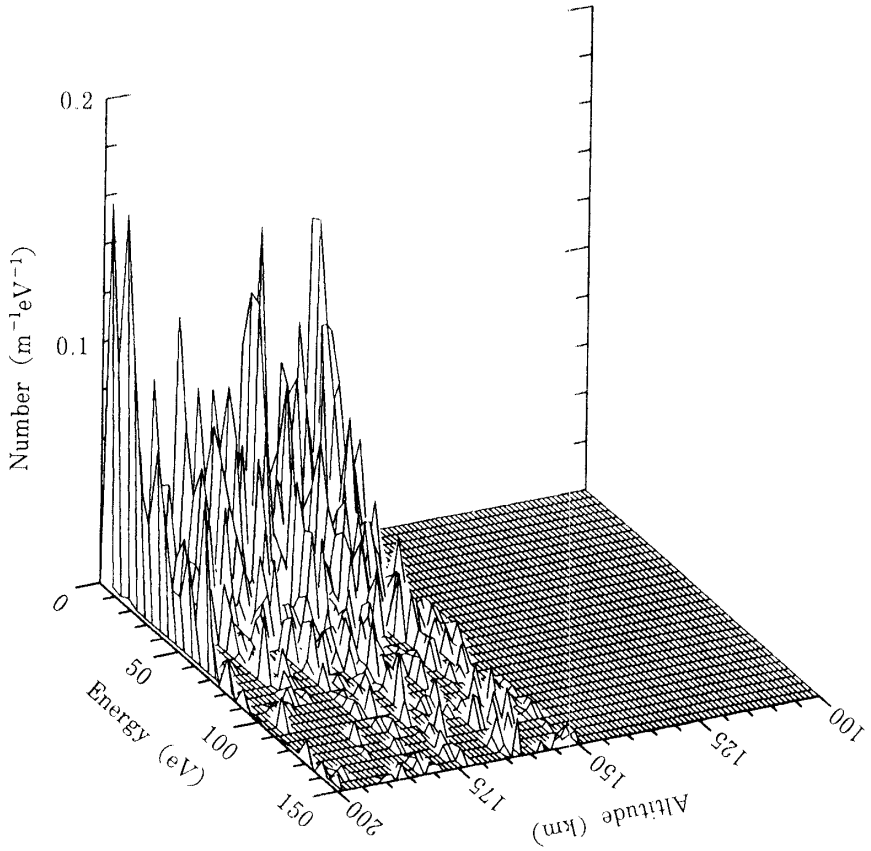

Fig. 6a. Energy and altitude distribution of the secondary electrons, normalized to one primary electron with $E_0 = 5$ keV. Angles are $\alpha = 0°$, $\beta = 30°$. 3 ms after the primary injection.

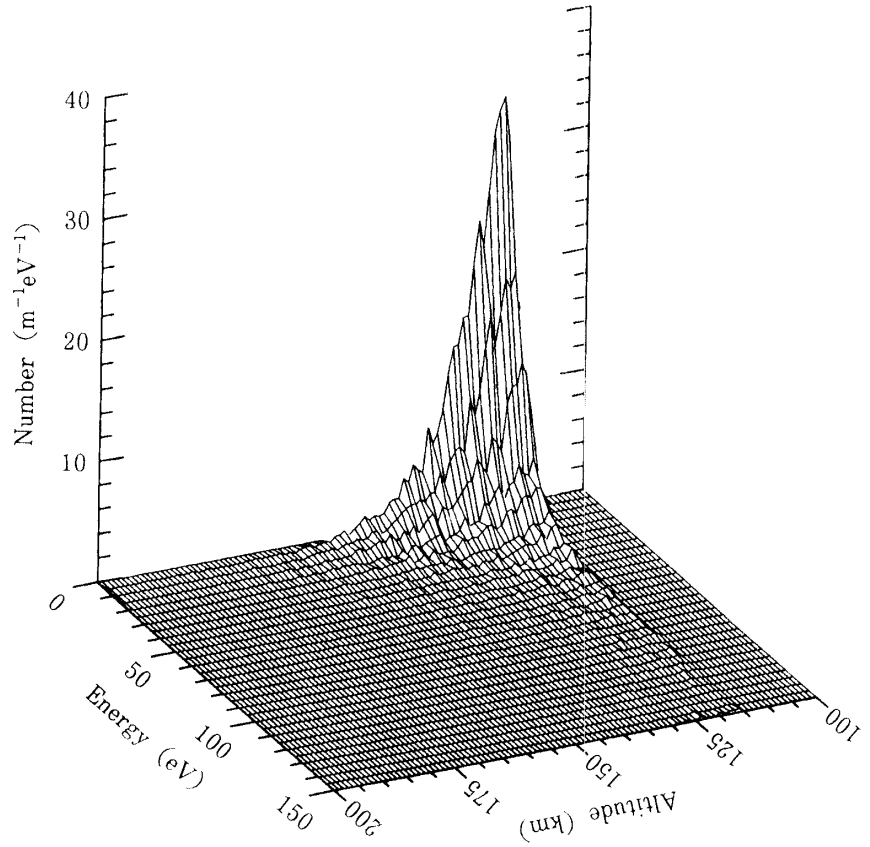

Fig. 6b. Same as Fig. 6a, but for 4 ms after the primary injection.

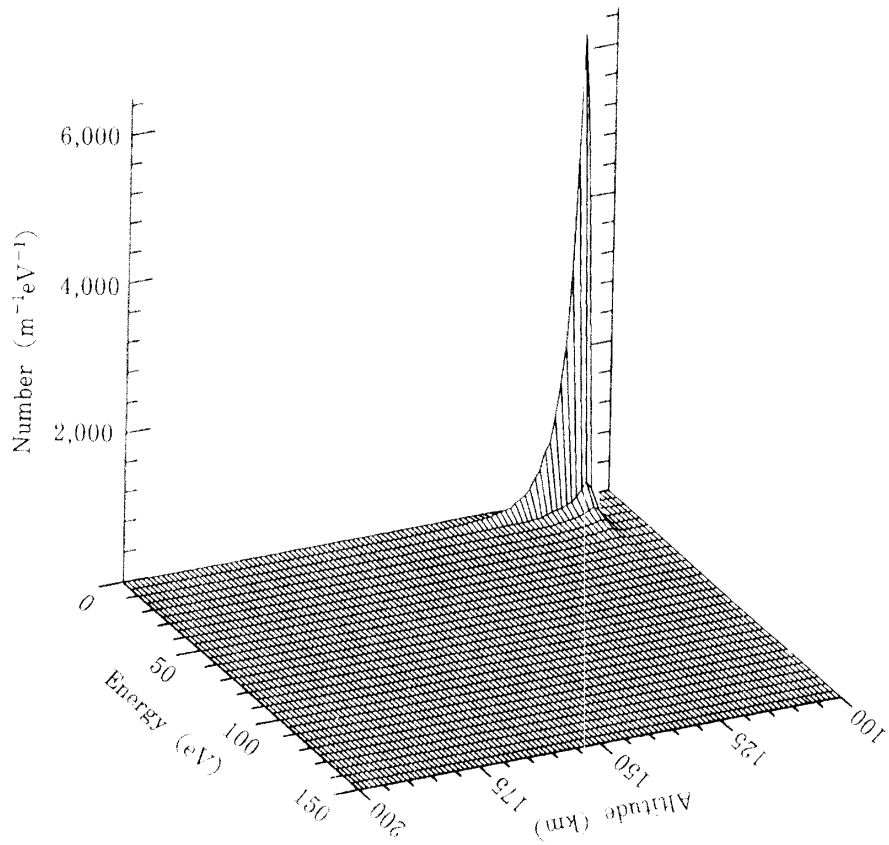

Fig. 6c. Same as Fig. 6a, but for 5 ms after the primary injection.

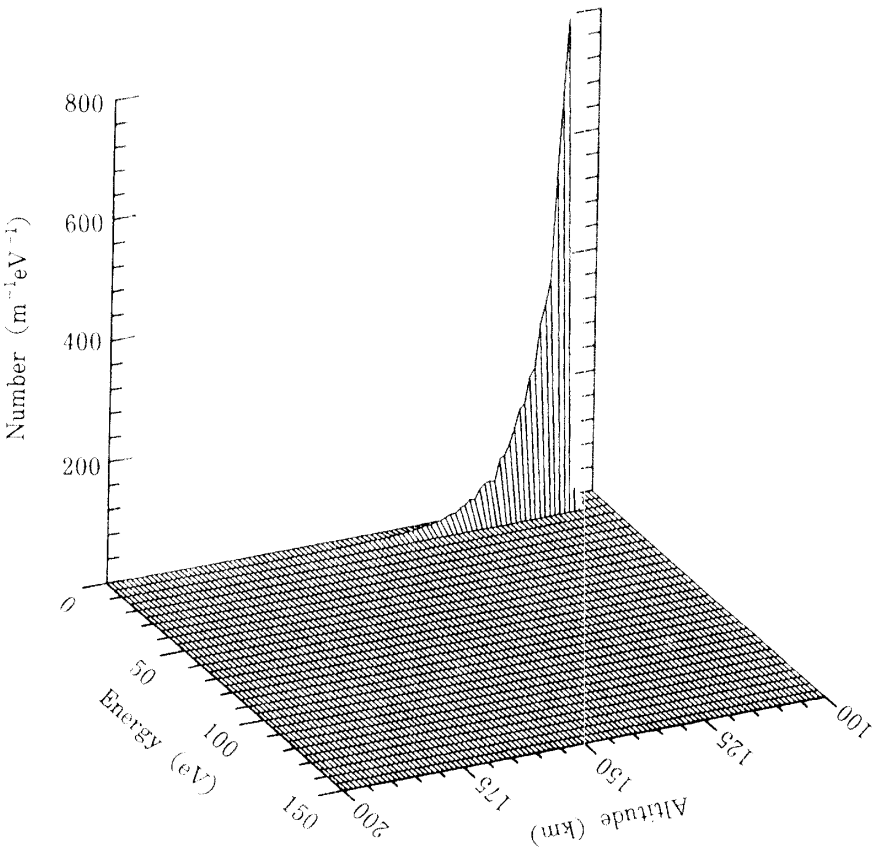

Fig. 6d. Same as Fig. 6a, but for 6 ms after the primary injection.

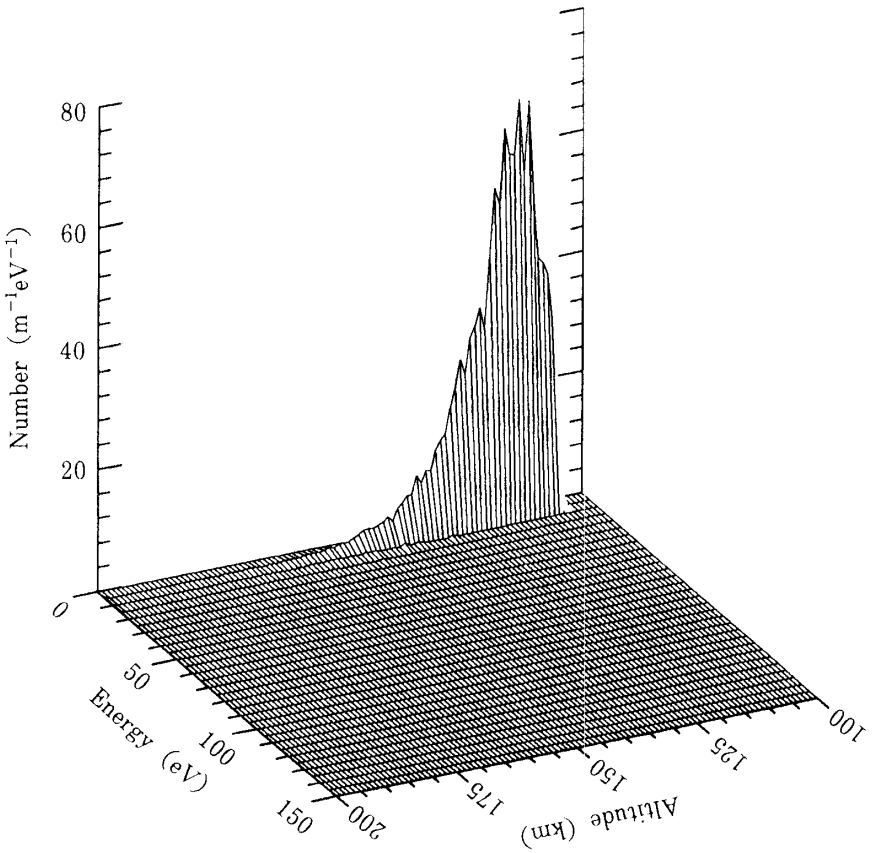

Fig. 6e. Same as Fig. 6a, but for 7 ms after the primary injection.

Figs. 6a, b, c, d and e show the corresponding energy and altitude distributions of the secondary electrons at 3, 4, 5, 6 and 7 ms after the primary injection. As in Fig. 5, the smoothing has not been achieved at 3 ms. Please note that here again the ordinate scale changes from Fig. 6a to Fig. 6e. In Fig. 6e, for instance, there is a peak which looks fairly large. But the absolute value is rather small. This figure does not mean that the secondary electrons are being produced at this instance. Figs. 6d and 6e indicate that the secondary electrons become quickly thermalized in the lowest region (near 100 km), while electrons in higher altitudes remain energetic for some time.

3.3 Dependence on the Angles α and β

In order to see the consequence of the increased pitch angle α, Figs. 7a, b, c, d and e show the resulting energy and altitude distributions of the primary electrons for $\alpha = 60°$, $\beta = 30°$ and the initial energy $E_0 = 5$ keV. (a) – (e) correspond, respectively, 5, 6, 7, 8 and 9 ms after the injection. The precipitating electrons now draw spiral orbits. The path length is twice as much as compared with the case of zero pitch angle for the same altitude drop. Therefore, it takes a longer time for these electrons to come down to the altitude level of, say, 120 km. Generally, the increase in α and β leads to the path length increase in proportion to sec α·sec β for a given altitude drop. It is also noted that for a given initial energy, electrons cannot penetrate into deeper atmospheres when sec α·sec β is large.

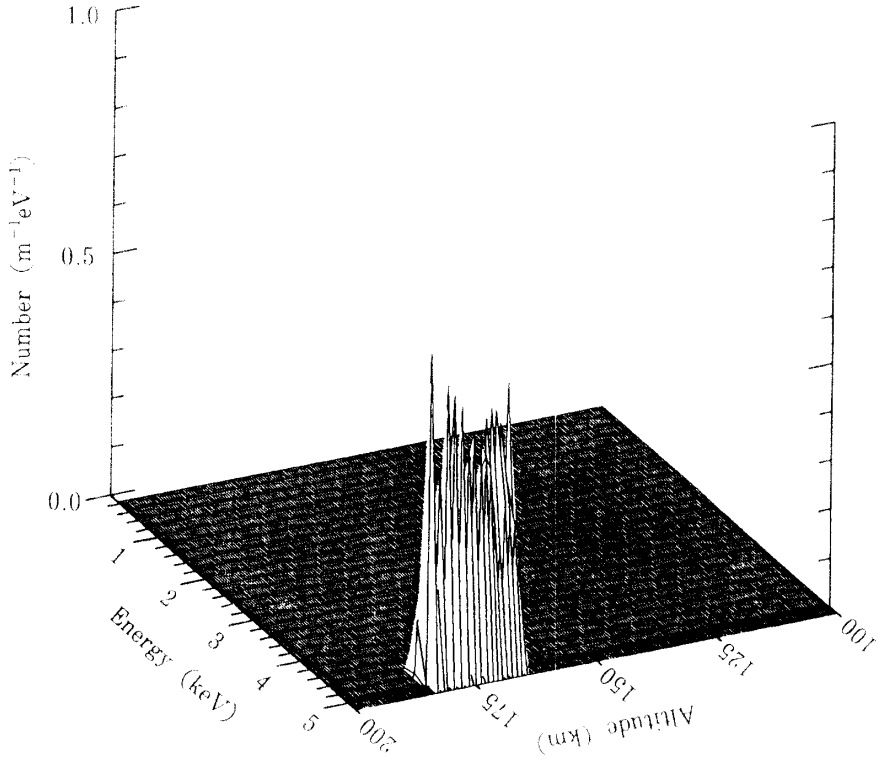

Fig. 7a. Energy and altitude distribution of the primary electrons injected with $E_0 = 5$ keV. Angles are $\alpha = 60°$, $\beta = 30°$. Distribution has been normalized to one electron. 5 ms after the injection at 250 km.

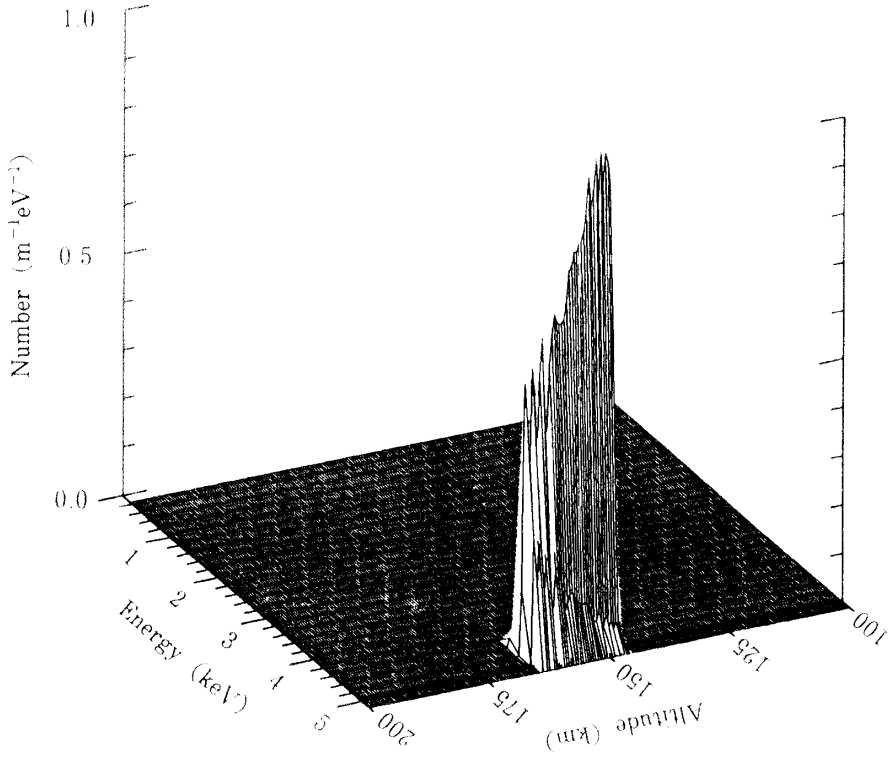

Fig. 7b. Same as Fig. 7a, but for 6 ms after the injection.

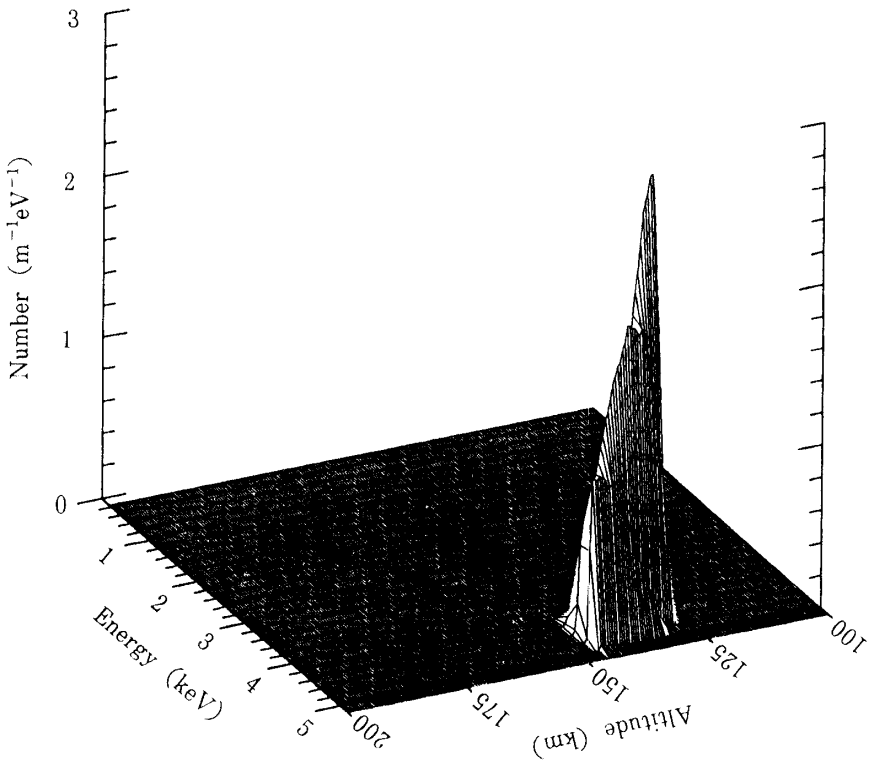

Fig. 7c. Same as Fig. 7a, but for 7 ms after the injection.

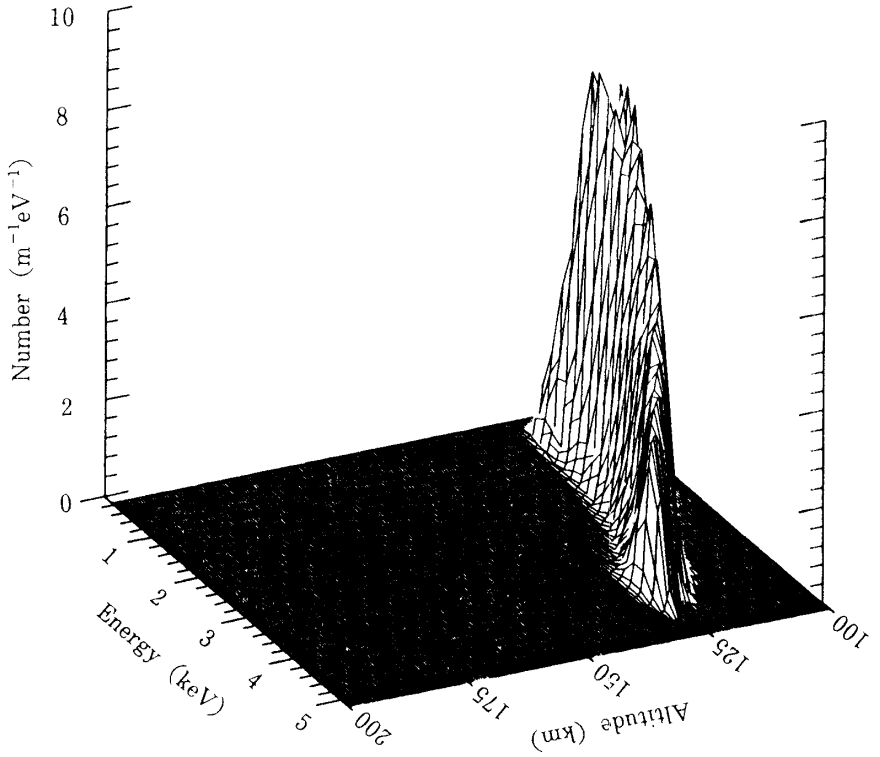

Fig. 7d. Same as Fig. 7a, but for 8 ms after the injection.

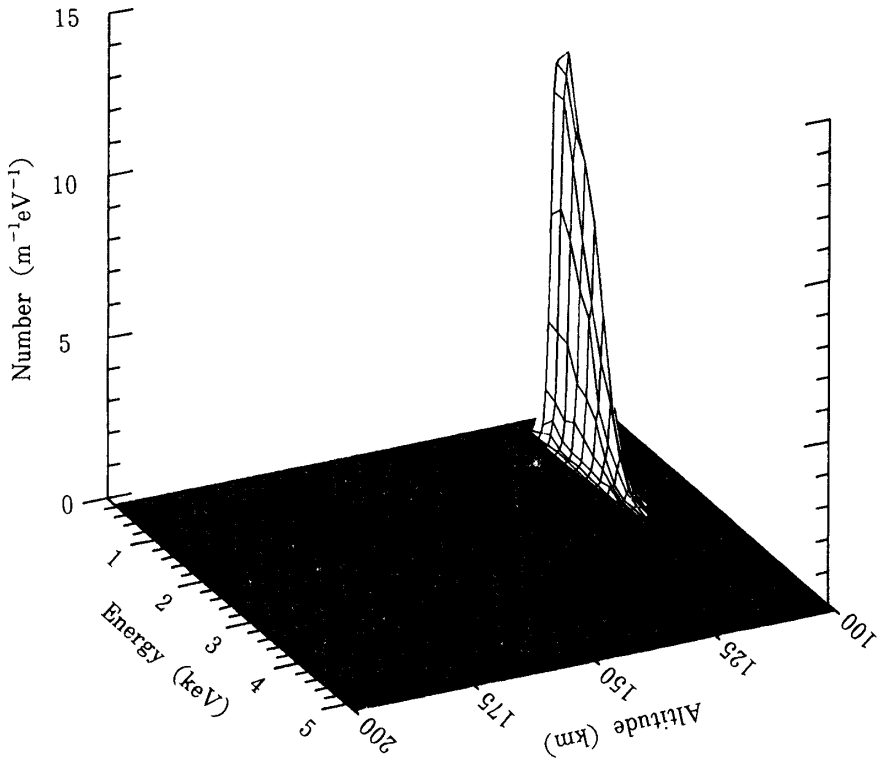

Fig. 7e. Same as Fig. 7a, but for 9 ms after the injection.

Figs. 8a and 8b show the profiles of the electron number density as a function of the altitude at several instances after the primary injection. Although the primary electron is also included, these curves practically represent the height distribution of the secondary electrons produced by the primary electron. (a) is for $\alpha = 0°$ and (b) is for $\alpha = 60°$. $E_0 = 5$ keV and $\beta = 30°$ are common to both figures. Curves are normalized to one primary electron. As in Figs. 5a and 6a, the distribution looks unnatural in early stages. In Fig. 8a, curves are shown only up to 5 ms after the injection. However, there is no further appreciable increase of the ionization after this instance. Similarly, in Fig. 8b, the ionization almost stops at 9 ms after the primary injection.

We have studied so far only the two sets of angle parameters, i.e., (α, β) = (0°, 30°) and (60°, 30°). We also studied two other cases: (α, β) = (0°, 60°) and (60°, 60°). For these four cases, the number of events per primary electron with $E_0 = 5$ keV is shown in Table 5 for some major processes. From these numbers, one can estimate, at least roughly, the number of events for other sets of (α, β). It is noted, however, that one cannot increase β further, because we have assumed that the atmospheric structure is plane-parallel. It is seen in Table 5 that as α and β increase, the number of collisions with N_2 and O_2 generally decreases, while the number of collisions with O increases. This is because for larger α and β the primary electrons spend most of the energy in the higher atmospheres where atomic oxygen is dominant.

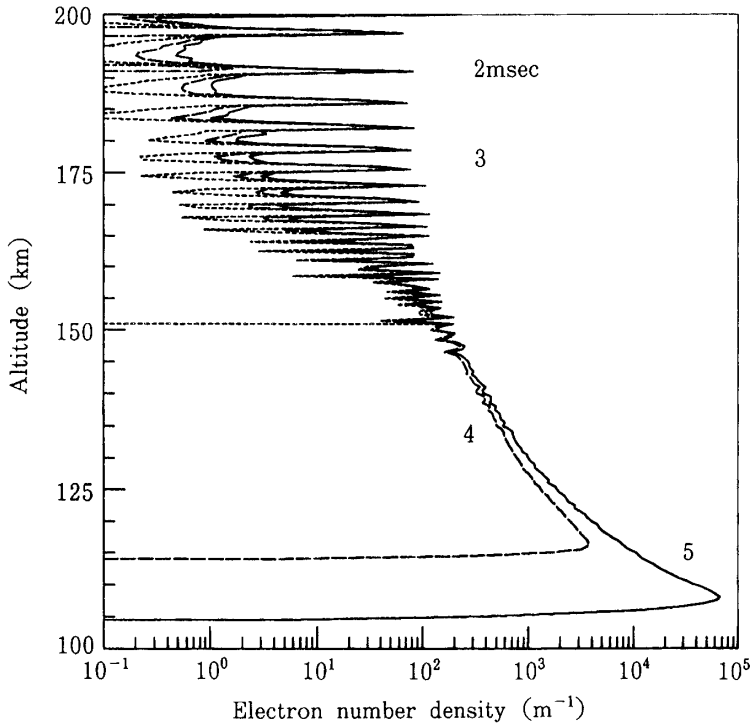

Fig. 8a. Altitude distribution of electrons produced by the precipitating electrons at 2, 3, 4 and 5 ms after the primary injection. Normalized to one primary electron. E_0 = 5 keV, α = 0°, β = 30°.

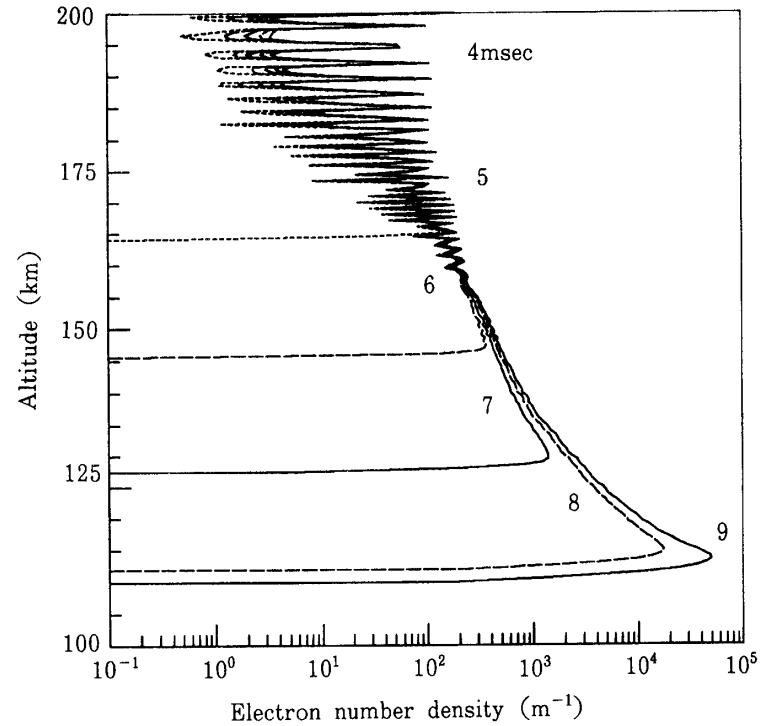

Fig. 8b. Same as Fig. 8a, but for α = 60°. 4, 5, 6, 7, 8 and 9 ms after the primary injection.

3.4 Dependence on the Initial Energy E_0

For $\alpha = 0°$, $\beta = 30°$, calculations have been done also for the initial electron energy $E_0 = 3$ keV and 7.5 keV in addition to $E_0 = 5$ keV. Comparison between these three cases with different E_0 values is presented in Table 6, where the number of events per primary electron is shown for various processes. As is expected, the number of events for each collision process increases as E_0 is increased. Exceptional behavior is found in atomic oxygen, where the number of each excitation or ionization process decreases slightly when E_0 increases from 5 to 7.5 keV. The reason is that at 7.5 keV the incident electrons come down quickly to lower atmospheres before losing appreciable energy and that in the lower atmospheres N_2 is more abundant than atomic oxygen.

Table 5. Number of some major collision processes per primary electron with $E_0 = 5$ keV. Dependence on angles α and β.

(a) Collisions with N_2

processes*) \ (α, β)	(0°, 30°)	(0°, 60°)	(60°, 30°)	(60°, 60°)
MT	6.99(3)	6.31(3)	6.10(3)	5.46(3)
vib. 0 → 1	3.50(1)	3.11(1)	3.01(1)	2.67(1)
vib. 0 → 2	1.34(1)	1.19(1)	1.15(1)	9.97
$A^3\Sigma^+_u$	2.74(1)	2.61(1)	2.63(1)	2.50(1)
$B^3\Pi_g$	2.08(1)	2.01(1)	2.01(1)	1.96(1)
$W^3\Delta_u$	1.18(1)	1.17(1)	1.17(1)	1.14(1)
$a^1\Pi_g$	1.37(1)	1.38(1)	1.36(1)	1.33(1)
$C^3\Pi_u$	8.46	8.23	8.31	8.12
HSS	6.13(1)	6.03(1)	5.97(1)	5.81(1)
$N_2^+(X^2\Sigma^+_g)$	4.47(1)	4.33(1)	4.33(1)	4.15(1)
$N_2^+(A^2\Pi_u)$	6.72(1)	6.59(1)	6.49(1)	6.34(1)
$N_2^+(B^2\Sigma^+_u)$	1.21(1)	1.19(1)	1.19(1)	1.14(1)
total number of collisions	7.32(3)	6.63(3)	6.41(3)	5.76(3)

(b) Collisions with O

processes*) \ (α, β)	(0°, 30°)	(0°, 60°)	(60°, 30°)	(60°, 60°)
MT	8.11(2)	9.55(2)	9.92(2)	1.16(3)
$(2p)^4\ ^1D$	4.67(1)	5.44(1)	5.62(1)	6.51(1)
$(2p)^4\ ^1S$	2.66	3.17	3.32	3.86
$(2p)^3 3s\ ^3S$	1.53	1.91	2.12	2.67
$(2p)^3 3p\ ^3p$	1.77	2.34	2.46	3.09
O^+	2.20(1)	2.78(1)	2.96(1)	3.70(1)
total number of collisions	8.87(2)	1.05(3)	1.09(3)	1.27(3)

(c) Collisions with O_2

processes*) \ (α, β)	(0°, 30°)	(0°, 60°)	(60°, 30°)	(60°, 60°)
MT	7.13(2)	6.05(2)	5.72(2)	4.71(2)
vib. 0 → 1	1.20(1)	1.05(1)	9.88	8.30
vib. 0 → 2	5.09	4.39	4.16	3.65
$a^1\Delta_g$	9.13	7.66	7.31	6.21
$b^1\Sigma_g^+$	2.13	1.75	1.70	1.41
A+C+c	3.96	3.78	3.50	3.01
$B^3\Sigma_u^-$	8.60	7.95	7.71	7.01
O_2^+	2.19(1)	2.00(1)	1.95(1)	1.72(1)
total number of collisions	7.77(2)	6.63(2)	6.27(2)	5.20(2)

*) "*vib.*" stands for the vibrational excitation. Other abbreviations are the same as in Table 4.

Table 6. Number of some major collision processes per primary electron. Energy dependence for $\alpha = 0°$ and $\beta = 30°$.

(a) Collisions with N_2

processes*)	$E_0 = 3$	5	7.5 keV
MT	3.08(3)	6.99(3)	1.14(4)
vib. 0 → 1	1.54(1)	3.50(1)	7.54(1)
vib. 0 → 2	7.42	1.34(1)	5.54(1)
$A^3\Sigma_u^+$	1.61(1)	2.74(1)	4.08(1)
$B^3\Pi_g$	1.20(1)	2.08(1)	3.03(1)
$W^3\Delta_u$	7.09	1.18(1)	1.84(1)
$a^1\Pi_g$	8.31	1.37(1)	2.08(1)
$C^3\Pi_u$	4.86	8.46	1.22(1)
HSS	3.64(1)	6.13(1)	9.27(1)
$N_2^+(X^2\Sigma_g^+)$	2.54(1)	4.47(1)	6.84(1)
$N_2^+(A^2\Pi_u)$	3.86(1)	6.72(1)	1.03(2)
$N_2^+(B^2\Sigma_u^+)$	7.12	1.21(1)	1.85(1)
total number of collisions	3.26(3)	7.32(3)	1.20(4)

(b) Collisions with O

processes*)	$E_0 = 3$	5	7.5 keV
MT	5.64(2)	8.11(2)	7.91(2)
$(2p)^4\ ^1D$	3.17(1)	4.67(1)	4.60(1)
$(2p)^4\ ^1S$	1.98	2.66	2.61
$(2p)^3 3s\ ^3S$	1.48	1.53	1.26
$(2p)^3 3p\ ^3P$	1.76	1.77	1.64
O^+	1.91(1)	2.20(1)	2.10(1)
total number of collisions	6.22(2)	8.87(2)	8.65(2)

(c) Collisions with O_2

processes*)	E_0 = 3	5	7.5 keV
MT	2.83(2)	7.13(2)	1.34(3)
vib. 0 → 1	5.35	1.20(1)	2.34(1)
vib. 0 → 2	2.33	5.09	9.52
$a^1\Delta_g$	3.56	9.13	1.73(1)
$b^1\Sigma_g^+$	7.95(−1)	2.13	3.94
A+C+c	2.14	3.96	6.98
$B^3\Sigma_u^-$	4.51	8.60	1.55(1)
O_2^+	1.10(1)	2.19(1)	3.96(1)
total number of collisions	3.14(2)	7.77(2)	1.46(3)

*) Abbreviations are the same as in Table 4 and 5.

3.5 Number of Electron-Ion Pair Productions and Number of Some Photo-Emissions

Figs. 9a and 9b show the number of electron-ion pair productions (ionization processes) per primary electron as a function of the altitude. Solid lines represent the results of the Monte Carlo calculations. For dashed curves see the next subsection. Here and also in the following three sets of figures, (a) is for $\alpha = 0°$ and (b) is for $\alpha = 60°$, both for $E_0 = 5$ keV and $\beta = 30°$.

Solid lines in Figs. 10a and 10b show the number of emissions in the first negative band system of nitrogen [N_2^+: $B^2\Sigma_u^+ \rightarrow X^2\Sigma_g^+$] per primary electron. Since the upper state of this transition immediately decays by emitting a photon, there is no collisional quenching effect to be taken into account. The excitation of the (0, 0) band emission with the wavelength around 3914 A is nearly 65% of the total excitation of the *B* state.

Solid lines in Figs. 11a and 11b show the number of emissions of the oxygen green line [O: $(2p)^4\ ^1S \rightarrow\ ^1D$ with wavelength ~ 5577 A] per primary electron. The upper state of this transition has a radiative lifetime of 0.79 s. Only about 6% of the oxygen atoms in this state is quenched by collision before emission. (See the reference [*3*], particularly the note added in proof in p. 31.)

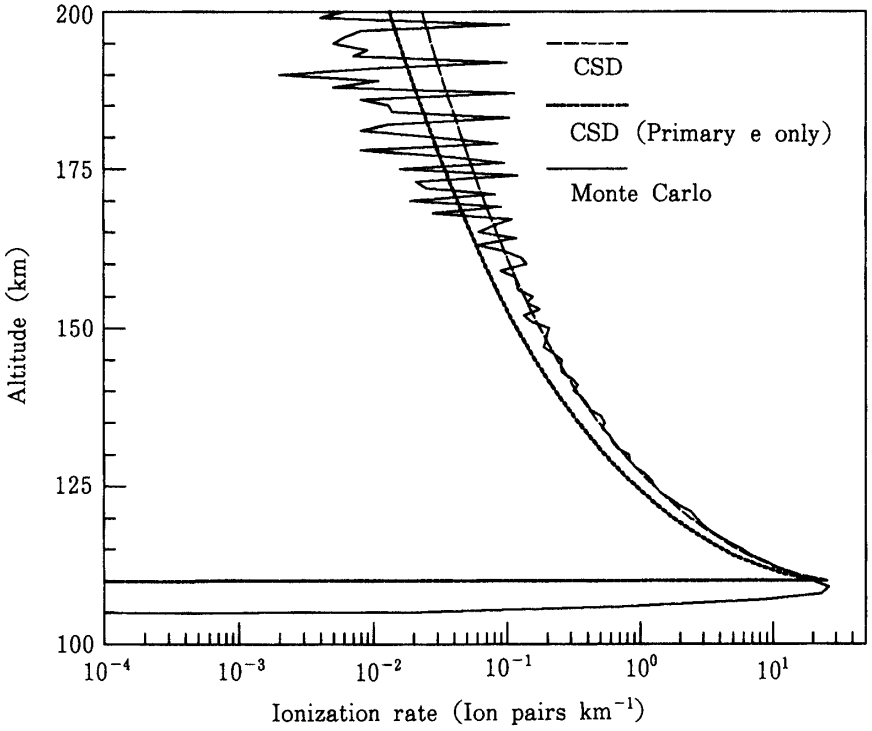

Fig. 9a. Altitude distribution of the ion-electron pair productions per primary electron. E_0 = 5 keV, α = 0°, β = 30°. Monte Carlo result is compared with CSD approximation. A CSD calculation, neglecting the secondary electron contribution, is also shown.

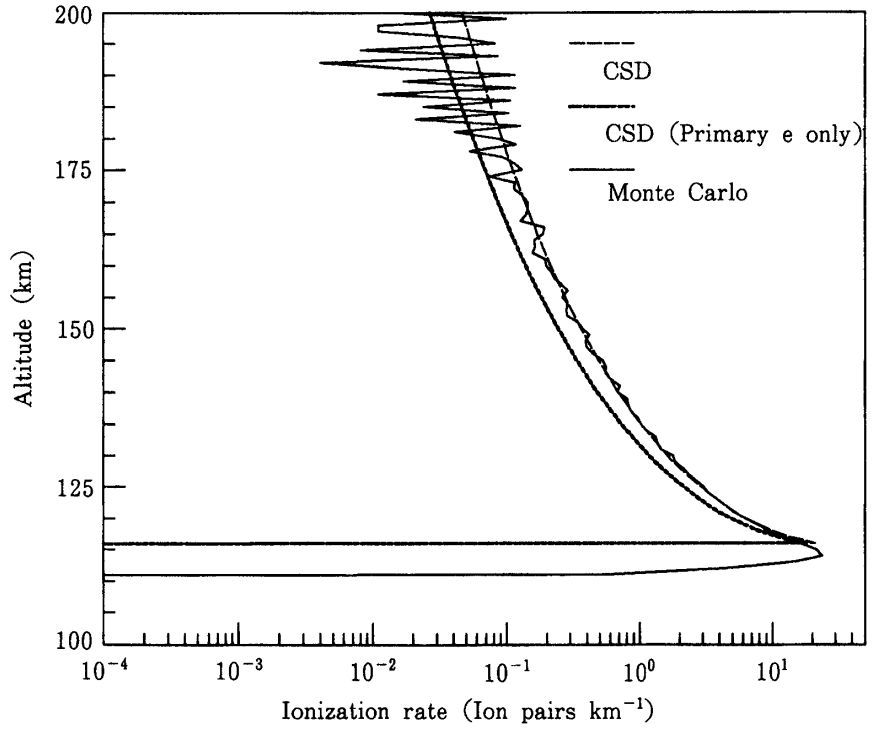

Fig. 9b. Same as Fig. 9a, but for α = 60°.

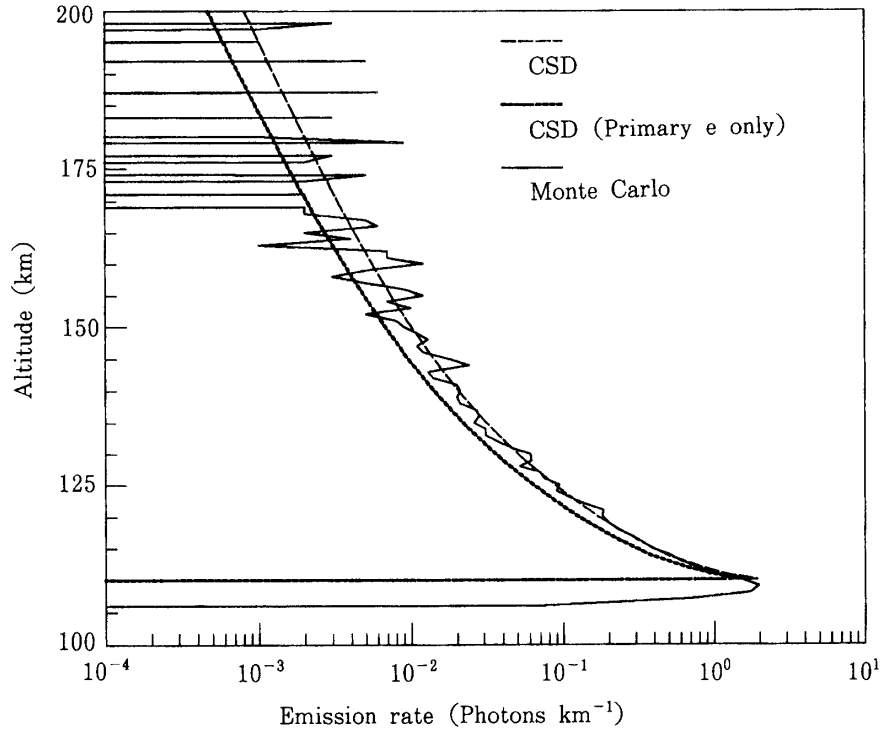

Fig. 10a. Altitude distribution of the photon emissions of the first negative band system of N_2^+ per primary electron. E_0 = 5 keV, α = 0°, β = 30°. Monte Carlo result is compared with CSD approximation. A CSD calculation, neglecting the secondary electron contribution, is also shown.

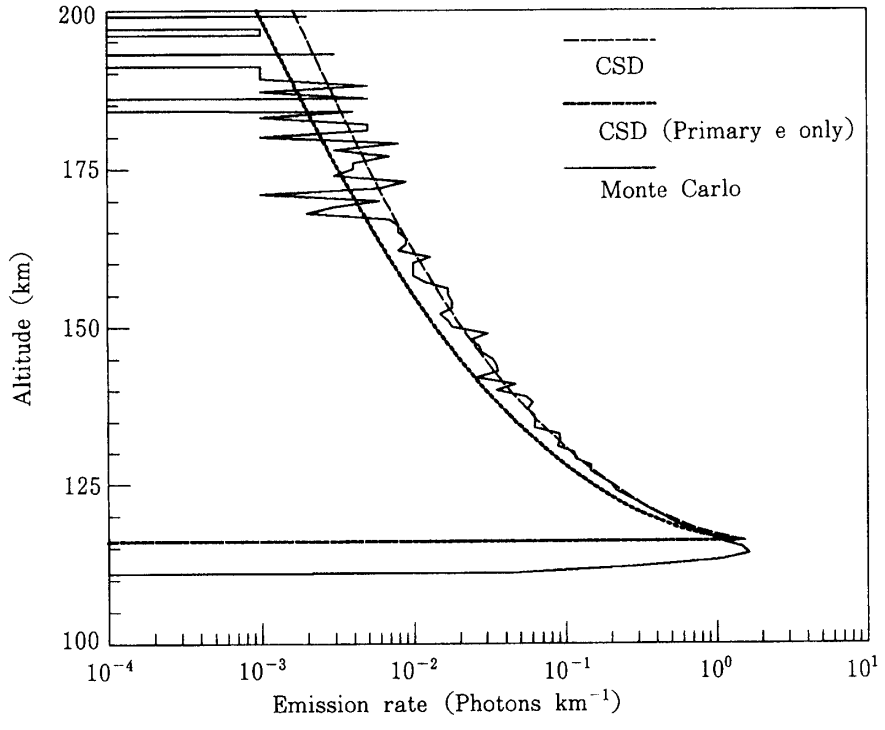

Fig. 10b. Same as Fig. 10a, but for α = 60°.

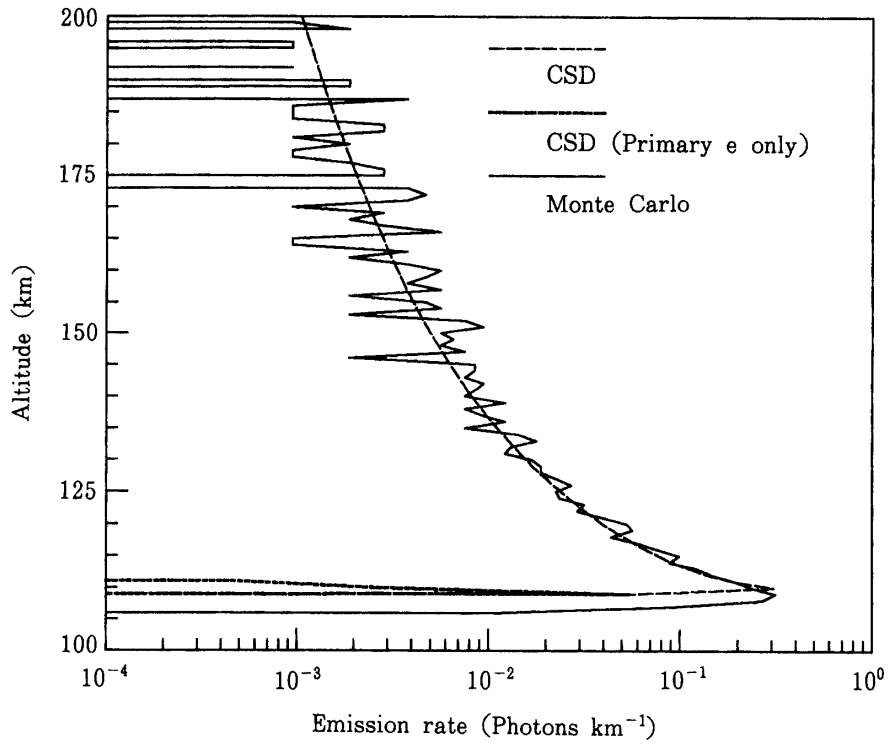

Fig. 11a. Altitude distribution of the photon emissions of the oxygen green line. E_0 = 5 keV, α = 0°, β = 30°. Monte Carlo result is compared with CSD approximation. A CSD calculation, neglecting the secondary electron contribution, is also shown.

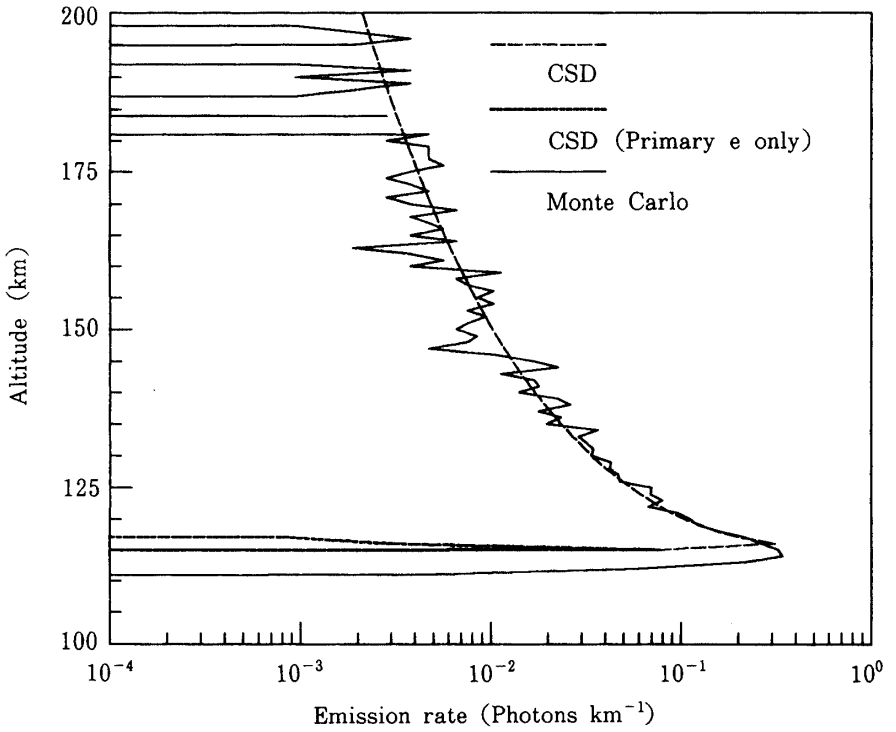

Fig. 11b. Same as Fig. 11a, but for α = 60°.

Solid lines in Figs. 12a and 12b show the number of excitations of atomic oxygen to $(2p)^4\ ^1D$ state and the number of emissions of the oxygen red line [O: $^1D_2 \rightarrow {}^3P_{0,1,2}$ with wavelengths ~ 6300 A] per primary electron. The big separation between these two curves in each figure comes from the collisional quenching before emitting radiation. The ^1D state of atomic oxygen has a lifetime of $\tau(^1D) = 147$ s. Because of the collisional quenching, the effective lifetime τ_{eff} is much shorter than $\tau(^1D)$. It is given by

$$\frac{1}{\tau_{eff}} = \frac{1}{\tau(^1D)} + \sum_j N_j(h)\ k_j(T(h)),\ (j = N_2,\ O_2), \tag{23}$$

where k_j is the rate coefficient of quenching in collision with atmospheric particle of the jth kind. For these coefficients, experimental data reported by Streit *et al.* [*16*] can be used. The numerical values of τ_{eff} in several altitudes are given in Table 7. Finally, the number of red-line photons emitted per primary electron is given in Table 8 for the four sets of angle parameters (α, β).

Table 7. Effective lifetime of $O(^1D)$

altitude (km)	$\tau_{eff}(^1D)$ (S)
120	0.081
140	0.726
160	2.91
180	8.42
200	20.4

Table 8. Total number of the oxygen red line photons emitted per primary electron ($E_0 = 5$ keV)

(α, β)	(0°, 30°)	(0°, 60°)	(60°, 30°)	(60°, 60°)
Number of photons	48.6	92.3	109.8	202.1

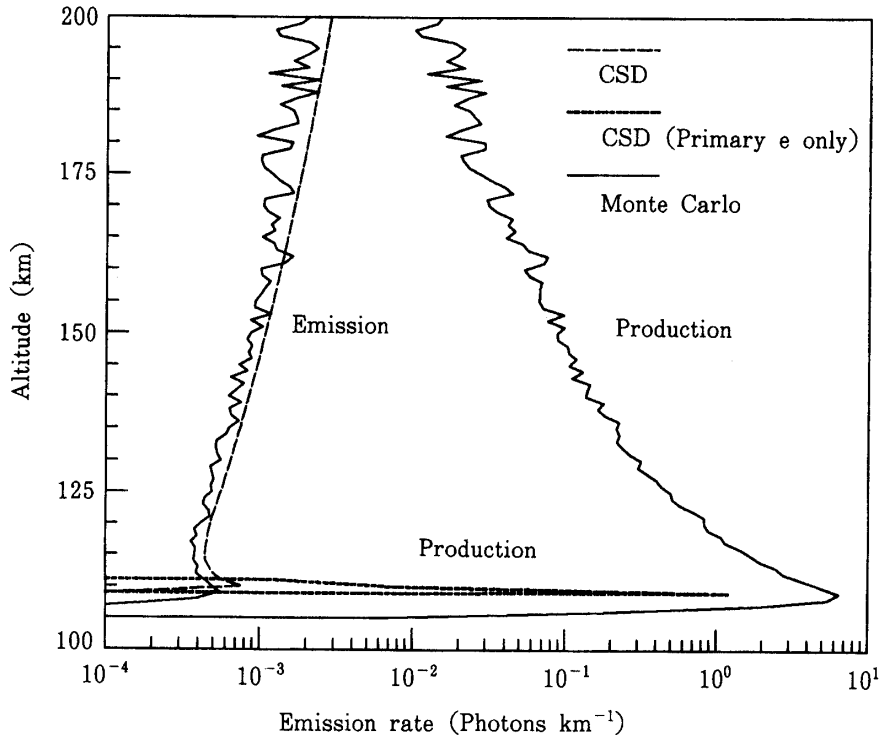

Fig. 12a. Altitude distribution of the $O(^1D)$ production and the emission of oxygen red line, both per primary electron. For the $O(^1D)$ production, the CSD estimation of the direct contribution of the primary electron is also shown. For the emission rate, the CSD approximation for the total rate, including both the primary and the secondary electron contributions, is also shown. $E_0 = 5$ keV, $\alpha = 0°$, $\beta = 30°$.

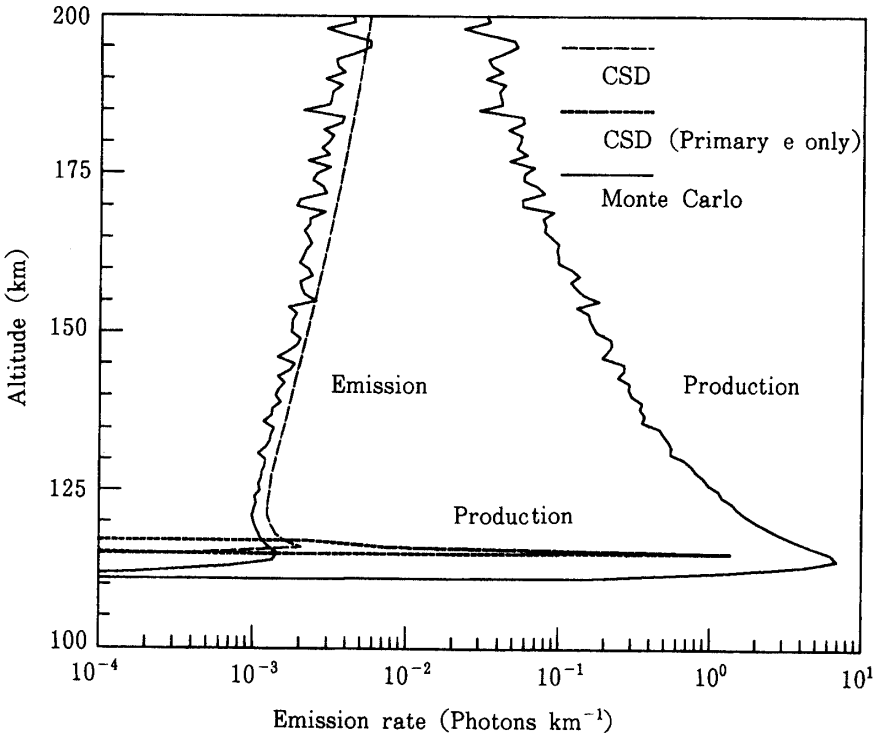

Fig. 12b. Same as Fig. 12a, but for $\alpha = 60°$.

3.6 Comparison with CSD Calculations

In Figs. 9-12, dashed and dotted curves are shown together with the Monte Carlo calculations represented by the solid lines. The dashed curves represent the corresponding results obtained in the CSD (continuous-slowing-down) approximation. For all the processes studied, the agreement between the Monte Carlo calculations and the CSD calculations is remarkably good, except in the lower boundary region.

The dotted curves represent the contributions from the primary electron, which have been estimated in the CSD approximation. For ionization and the excitation of the nitrogen first negative bands, the primary electron contributes to more than 50% of the total (primary plus secondary contributions). However, for the two excitations of atomic oxygen, the primary electron contributes very little. Its contribution is localized toward the lowest altitude region. This is because the excitation of the ^{1}D and ^{1}S states of atomic oxygen is appreciable only in the low collision energies (less than about 100 eV). The contribution of the secondary electrons dominates here.

4. Summary and Discussions

We have studied the electron precipitation from the altitude of 250 km, producing excitation of some photon emissions and ionizations. Unless the pitch angle α of the electron motion or the angle β (the inclination of the geomagnetic field is $90° - \beta$) or both are large, the time scale of the precipitation is roughly 5 ~ 10 milliseconds. After this period of time, the primary electrons have lost most of their energy and reach the altitude around 105 ~ 110 km, depending on α and β. If α is very large (near 90°), it takes much longer time for electrons to come down to lower atmospheres. For a large β, our model cannot be applied because we have assumed that the structure of the atmosphere is plane-parallel. For other combinations of α and β, one can estimate the number of various events, at least roughly, by interpolating or extrapolating the values listed in Table 5.

If the electron injection takes place at higher altitudes, say 300 km, we may assume to the first approximation that electrons have no collision until they come down to the level of 250 km. Then, the present results can be applied.

We have not discussed the horizontal spreading of the electron distribution. In an artificial aurora experiment, an electron beam of some strength will be injected into the atmosphere. First, we have to take account of the motion of the space vehicle where the electron gun is installed. In the circular orbit with the altitude of 250 km, the vehicle should have a horizontal speed around 8 km/s. This has a large influence on the spatial shape of the artificial aurora produced by the experiment. Then, because of the space charge of the beam and also because of the diffusion caused by collisions, the beam will be spreading while the electrons are coming down.

We have studied the electron precipitation for the initial electron energy E_0 = 3, 5 and 7.5 keV. (See Table 6) Normally, when E_0 is increased, the number of excitations and ionizations is also increased. We have seen, however, slight deviations from this general trend in atomic oxygen. For the values of E_0 not found in Table 6, one may interpolate or extrapolate the values in the table. This table is for $\alpha = 0°$ and $\beta = 30°$. Thus, further approximate interpolation or extrapolation based on Table 5 is necessary for other sets of α and β.

For the altitude distribution of various excitation and ionization processes studied, we have seen in Figs. 9-12 that the agreement between the Monte Carlo calculation and the CSD approximation is remarkably good, except in the lowest region of the altitude. In the lowest altitude (around 105 ~ 110 km), the CSD distribution has a sharp cutoff, while the Monte Carlo result extends further to lower altitudes. This is because the CSD calculation describes the precipitation of *one* electron with averaged behavior. Needless to say, the Monte Carlo results are more realistic. However, the CSD calculations require much less computation time. If the accurate penetration depth for the precipitating electrons is not required, the CSD approach can be regarded as an appropriate way of calculations.

For the excitation of the first negative band system of N_2^+ and the ionization in general, the contribution of the primary electron and that of the secondary electrons are comparable. (See Figs. 9 and 10.) The first negative (0,0) band with the wavelength of 3914 A is one of the most prominent features in optical aurorae. To obtain the number of this photon from Figs. 10a and 10b, we have to multiply 0.642. The reason is that in the data compilation [*10*] adopted in the present work the cross section for production of $N_2^+(B)$ was obtained from the experimental cross section [*17*] of the first negative (0, 0) band emission by multiplying 1/0.642.

For excitation of the green and the red lines of atomic oxygen, the contribution of the secondary electrons is dominant because the relevant excitation cross sections have appreciable values only in the low energy region. The ^1S state of the atomic oxygen has a radiative lifetime of 0.79 s. Quenching effects exist, but not so large. The effective lifetime for the emission of 5577 A photon is about 0.75 s. The effective lifetime gives a measure of the period of time during which emission can be seen, provided that the incident electron flux is sufficiently large. The ^1D state of the atomic oxygen, on the other hand, has a much longer radiative lifetime (147 s.), during which the collisional quenching can easily take place, particularly in the lower atmospheres where the number density is higher. It is seen in Figs. 12a and 12b that only about 0.01% of the $O(^1D)$ atoms produced by the electron precipitation can actually emit the red line (about 6300 A) photons in the lowest altitudes of our interest. The emission rate is higher at higher altitudes. There, the effective lifetime is 1 ~ 20 s. (See Table 7.) Because of this quenching effect, the total number of red-line photo-emissions depend considerably on the angles α and β. (See Table 8.) It may be added that during the effective lifetime, the metastable $O(^1D)$ atoms can move a few km away in the high altitude regions from the spot where it

was created.

The metastable atoms $O(^1D)$ are also produced through some indirect ways. (See, for instance, Solomon *et al.* [*18*].) Among others, the dissociative recombination process

$$e + O_2^+ \rightarrow O(^1D) + O(^3P \text{ or } ^1D) \tag{24}$$

is probably the most important one. The recombination coefficient $\alpha_r(T_e)$ between the thermal electron and O_2^+ is about 2×10^{-7} cm^3/s at the electron temperature T_e = 300 K and becomes smaller at higher temperatures [*18*]. The quantum yield for the production of $O(^1D)$ has been estimated to be 1.2 [*18*]. In Fig. 13 the altitude distribution of the O_2^+ ions produced by the electron precipitation is shown. The number of O_2^+ produced is smaller than the number of direct production of $O(^1D)$ (Fig. 12a) by a factor of 3 ~ 10, depending on the altitude. Taking all these values, we can conclude that the indirect excitation of the oxygen red line is not negligible, but it does not give a drastic change in the $O(^1D)$ production rate which is basically given by the direct excitation. It is also noted that the recombination process takes some time. If we assume that the ionospheric electron density is $n_e = 10^5 - 10^6$ cm^{-3} and use the recombination coefficient α_r at 300 K, the production of $O(^1D)$ through the process (24) will continue for $\tau = 1/(\alpha_r n_e) = 5 - 50$ s. This is to be compared with the time scale of the order of 10 ms in the direct excitation of $O(^1D)$ by the precipitation electrons.

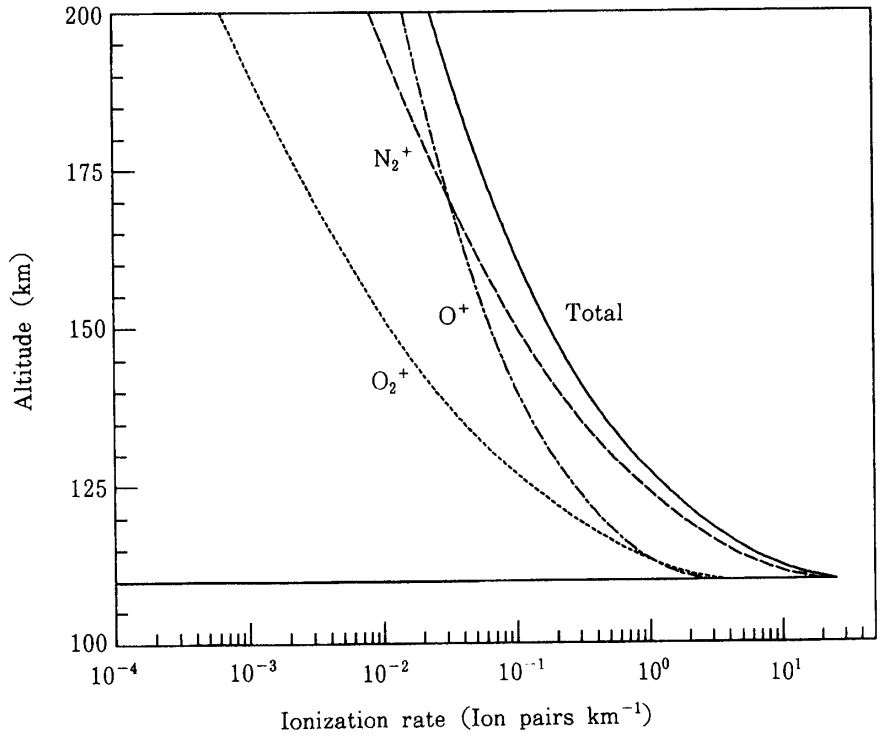

Fig. 13. Composition of ions produced by the electron precipitation. CSD calculation corresponding to Fig. 9a.

Finally, a few words must be added on the vibrational excitations of N_2 and O_2. Although we have shown the number of vibrational excitations in this article, these numbers correspond to the excitations by the electrons with energy higher than 5 eV. In reality, much more vibrational excitations will be produced by electrons after the energy becomes below 5 eV. Total number of the vibrationally excited species cannot be obtained without estimating the excitations by slow electrons.

Acknowledgments

A contribution of Mr. T. Nimura in an early stage of this work is gratefully acknowledged.

Numerical calculations have been done on FACOM M-780/20 and VP-200 at the Computer Center, ISAS.

References

[1] A. Vallance Jones and R.L. Gattinger, "Auroral spectroscopy and its application to the characterization of primary particle fluxes", *J. Geomag. Geoel.*, **42**, 1990, pp. 1385-1410.

[2] P.G. Richards and D.G. Torr, "Auroral modeling of the 3371 A emission rate: Dependence on characteristic electron energy", *J. Geophys. Res.*, **95**, No. A7, 1990, pp. 10,337-10,344, and references therein.

[3] K. Takayanagi, "A numerical study of artificial electron aurora experiment", *ISAS Report* **No. 611**, 1984, pp. 1-32.*)

[4] P.M. Banks, C.R. Chappell and A.F. Nagy, "A new model for the interaction of auroral electrons with the atmosphere: Spectral degradation, backscatter, optical emission, and ionization", *J. Geophys. Res.*, **79**, 1974, pp. 1459-1470.

[5] D.J. Strickland, D.L. Book, T.P. Coffey and J.A. Fedder, "Transport equation techniques for the deposition of auroral electrons", *J. Geophys. Res.*, **81**, 1976, pp. 2755-2764.

[6] K. Stamnes, "Analytic approach to auroral electron transport and energy degradation", *Planet. Space Sci.*, **28**, 1980, pp. 427-441.

[7] M.J. Berger, S.M. Seltzer and K. Maeda, "Some new results on electron transport in the atmosphere", *J. Atm. Terr. Phys.*, **36**, 1974, pp. 591-617.

[8] CIRA 1972 (COSPAR International Reference Atmosphere 1972), Akademie-Verlag (Berlin, 1972).

[9] C.B. Opal, W.K. Peterson and E.C. Beaty, "Measurements of secondary-electron spectra produced by electron impact ionization of a number of simple gases", J. *Chem. Phys.*, **55**, 1971, pp. 4100-4106; C.B. Opal, E.C. Beaty and W.K. Peterson, "Tables of secondary-electron production cross sections", Atomic Data **4**, 1972, pp. 209-253.

[10] Y. Itikawa, M. Hayashi, A. Ichimura, K. Onda, K. Sakimoto, K. Takayanagi, M. Nakamura, H. Nishimura and T. Takayanagi, "Cross sections for collisions of electrons and photons with nitrogen molecules", *J. Phys. Chem. Ref. Data* **15**, 1986, pp. 985-1010.

[11] Y. Itikawa, A. Ichimura, K. Onda, K. Sakimoto, K. Takayanagi, Y. Hatano, M. Hayashi, H. Nishimura and S. Tsurubuchi, "Cross sections for collisions of electrons and photons with oxygen molecules", *J. Phys. Chem. Ref. Data* **18**, 1989, pp. 23-42.

[12] Y. Itikawa and A. Ichimura, "Cross sections for collisions of electrons and photons with atomic oxygen", *J. Phys. Chem. Ref. Data* **19**, 1990, pp. 637-651.

[13] A. Chutjian, D.C. Cartwright and S. Trajmar, "Electron impact excitation of the electronic states of N_2. III. Transitions in the 12.5-14.2-eV energy-loss region at incident energies of 40 and 60 eV", *Phys. Rev.*, **A16**, 1977, pp. 1052-1060.

[14] S. Trajmar, D.F. Register and A. Chutjian, "Electron scattering by molecules II. Experimental methods and data", *Phys. Rept.*, **97**, 1983, pp. 219-356.

[15] A.V. Phelps and L.C. Pitchford, "Anisotropic scattering of electrons by N_2 and its effect on electron

transport", *Phys. Rev.*, **A31**, 1985, pp. 2932-2949.

[16] G.E. Streit, C.J. Howard, A.L. Schmeltekopf, J.A. Davidson and H.I. Schiff, "Temperature dependence of $O(^1D)$ rate constants for reactions with O_2, N_2, CO_2, O_3, and H_2O", *J. Chem. Phys.*, **65**, 1976, pp. 4761-4764.

[17] W.L. Borst and E.C. Zipf, "Cross section for electron-impact excitation of the (0,0) first negative band of N_2^+ from threshold to 3 keV", *Phys. Rev.*, **A1**, 1970, pp. 834-840.

[18] S.C. Solomon, P.B. Hays and V.J. Abreu, "The auroral 6300 A emission: Observations and modeling", *J.Geophys. Res.*, **93**, No. A9, 1988, pp. 9867-9882.

*) An error has been found in the computer program in the previous work [3]. All the values of time, such as those in the abscissae in Figs. 7-12, should be multiplied by two.